Mechanistic Model for Catalytic Recombination During Aerobraking Maneuvers

FINAL REPORT

NASA Grant NAG-9-314

Prepared by

Ronald J. Willey
Associate Professor
Northeastern University
Department of Chemical Engineering
Boston, MA

Prepared for

Mr. Stanley H. Goldstein, DPA
Director, University Programs
NASA
AHU
Lyndon B. Johnson Space Center
Houston, Texas 47058

Date Submitted

November 30, 1989

RJW/cv/014

TABLE OF CONTENTS

LIST OF TABLES

LIST OF FIGURES

LIST OF FIGURES Continued

LIST OF FIGURES Continued

ABSTRACT

Several mechanistic models are developed to predict recombination coefficients for use in heat shield design for reusable surface insulation (RSI) on aerobraking vehicles such as space shuttles. The models are applied over a temperature range of 300 to 1800 K and a stagnation pressure range of 0 to 3,000 Pa. A four parameter model in temperature was found to work best, however several models (including those with atom concentrations at the surface) were also investigated. Mechanistic models developed with atom concentration terms may be applicable when sufficient data becomes available. This work shows the requirement for recombination experiments in the 300 to 1000 K and 1500 to 1850 K temperature range, with deliberate concentration variations.

INTRODUCTION

The objective was to determine a continuous model for the recombination coefficients of atoms on space shuttle tiles and similar heat shield materials. This model could then be applied in heat shield design calculations used in reentry simulations, to help determine the amount and type of heat shield material required. Currently, the experimental data shows a maximum recombination rate at around 1600 K, accounted for by discontinuous recombination models which change at the maximum observed in the data. This work closely examines two mechanisms to determine if they can predict the observed recombination data over a wider range of temperatures. These mechanisms also demonstrate an influence of atom concentration on the recombination coefficients.

The results can be applied in heat shield calculations for the aeroassist flight experiment (AFE) and aero-orbiter transfer vehicle (AOTV). Higher reentry temperatures are predicted at the heat shield surfaces. However, current recombination models cannot predict observed recombination rates at higher temperatures. For instance, a simple Arrhenius model predicts heating rates two times higher than measured because the model predicts higher recombination coefficients than those observed. The use of a continuous model which reflects actual recombination data across a wider temperature range, will allow more flexibility in determining the best reentry pattern and heat shield design for space craft reentry systems.

Figure 1 from Ting et al. (1989) demonstrates the aeroassist flight experiment (AFE) which is proposed for 1993. This figure portrays how the aeroassist vehicle will travel through the atmosphere, simulating an aerobraking maneuver while returning to the space shuttle. It is during this aerobraking maneuver where recombination and heat shield design become important.

FIGURE 1

Aeroassist Flight Experiment (AFE) Mission Profile
(from Ting et al., 1989)

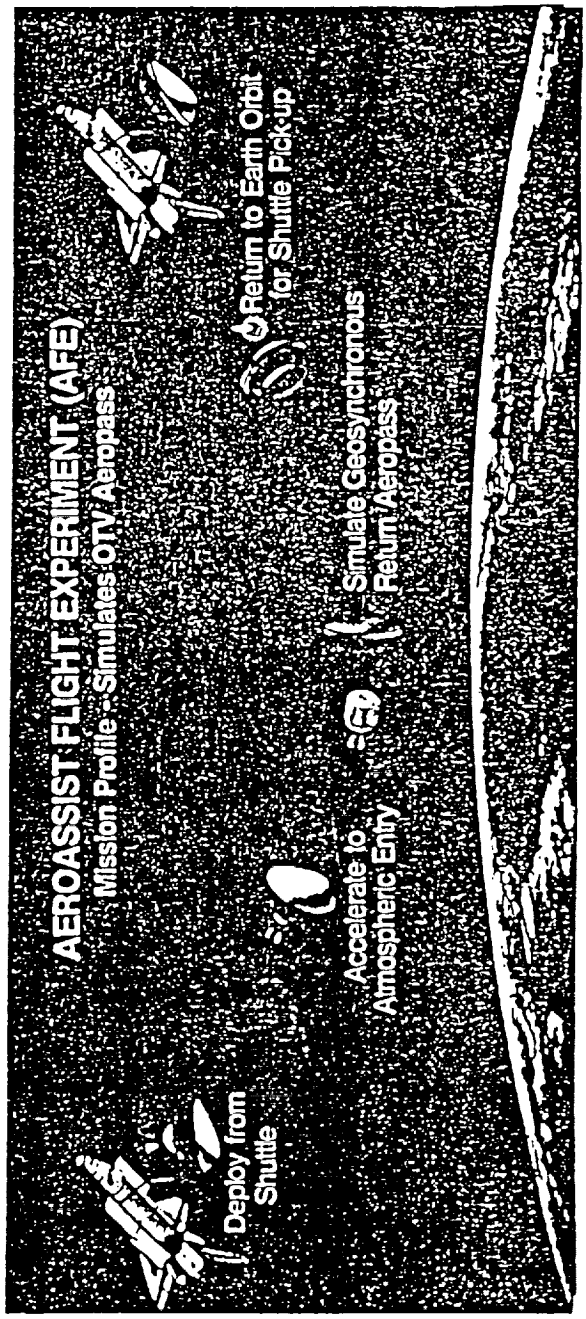

BACKGROUND

General Background

Space shuttle orbiter reentry experiments have shown that catalytic surface recombination influence heat shield temperatures (Scott, 1985). Specifically, increases up to 111 K have been reported for temperatures measured on a catalytically coated space shuttle tile in contrast to non-catalytically coated space shuttle tiles. The higher temperatures observed on catalytically coated tiles are explained by increased surface recombination of atoms to molecules. Further, Rosner & Fang (1974) suggested that recombination is not entirely to ground state molecules. For instance, molecules created by surface recombination at one point come off the surface excited, later transferring energy further downside the space craft surface. To date, mechanistic description of this phenomena has been lacking. Based on data presently available, a mechanistic model should be able to describe the maximum in the recombination coefficient as temperature increases. This maximum occurs around 1600 K based on available data.

Figure 2 demonstrates the reentry chemistry that occurs. As a vehicle reenters the atmosphere, a bow shock is established off the front nose of the vehicle. As flow goes across the bow shock, molecules are disassociated into atoms. These atoms then recombine on the surface, dumping their energy of recombination onto the surface, and leave the surface as molecules. The ideal surface would have four characteristics: 1) high emissivity, 2) low recombination rates, 3) the ability to withstand high temperatures, and 4) insulating capabilities to the vehicle itself. This report focuses on the description of recombination rates of atoms. To demonstrate the amount of energy released during recombination, it is important to note that the reaction of two oxygen atoms on the surface will release about 500 kJ/mole. This is equivalent to the energy released by the combustion of coal on a per unit mass basis. Similarly, recombination of nitrogen atoms releases about two times as much energy on the surface. Therefore, each pound of

FIGURE 2

Reentry Flow Field

(from Kolodziej and Stewart, 1987)

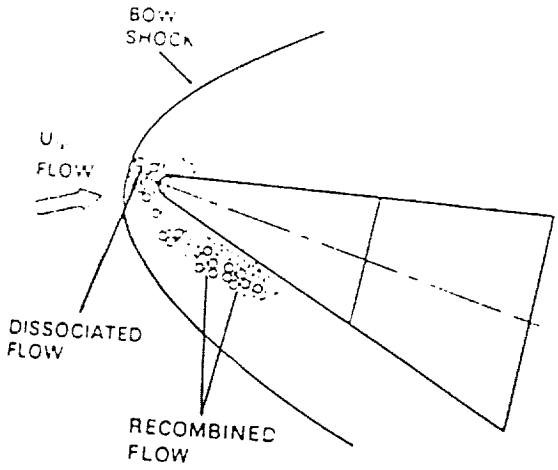

nitrogen atoms which recombine on the surface would be equivalent to burning two pounds of coal. Space shuttle tiles are composed of about 1" thick low density silica called "high temperature re-usable surface insulation" (HRSI) coated with about 3 millimeters thick reaction cured glass (RCG). RCG coating is an excellent non-catalytic surface and is ideal for the purpose of low recombination. However, some recombination continues to occur and must be accounted for in heat shield calculations.

Currently, recombination is accounted for by recombination coefficients which are the combination of two components. The first component is the probability that atoms will recombine when they collide on the surface. The second component, then, is the fraction of dissociation energy released to the surface. The recombination coefficients discussed in this report are thus called energy transfer catalytic recombination coefficients for nitrogen and oxygen. The ability to separate the probability of recombination from the fraction of dissociation energy released has yet to have been accomplished experimentally. However, mechanisms can still be used to describe the data. In general, recombination data is fitted to an Arrhenius expression:

$$\gamma = k \qquad (1)$$

where k consists of 2 parameters, k_o and Ea. The Arrhenius expression becomes:

$$k = k_0 \exp(-Ea/RT) \qquad (-1a)$$

where k_0 is called the pre-exponential coefficient and Ea is called the activation energy.

For example, Kolodziej & Stewart (1987) reported the recombination coefficient for nitrogen and oxygen as shown below. The Arrhenius expression changed at about 1600 K for nitrogen and oxygen, and specifically the activation energy changed from positive to negative.

$$\gamma_N = 6.1 \times 10^{-2} \exp(-2480/T_W) \qquad 1410 < T_W < 1640 \qquad (2)$$

$$\gamma_N = 6.1 \times 10^{-4} \exp(5090/T_W) \qquad 1640 < T_W < 1905 \qquad (3)$$

$$\gamma_O = 40 \exp(-11440/T_W) \qquad 1435 < T_W < 1580 \qquad (4)$$

$$\gamma_O = 39 \times 10^{-9} \exp(21410/T_W) \qquad 1580 < T_W < 1845 \qquad (5)$$

Recombination data taken over a wider range of temperature suggest that a simple Arrhenius expression will not work. For example, look at the recombination coefficient of nitrogen on silica in Figure 3 (Newman, 1987). Ignoring the wide range of data at 300 K, the figure shows that from a temperature range of about 300 to 1000 K a rather low activation energy exists (proportional to the negative slope of the line). As temperature increases from 1000 to about 1400 K the activation energy increases. Above 1400 K, the activation energy changes from positive to negative and gamma decreases.

The objective of this work is to describe the recombination coefficient over a wider temperature range with one equation.

Recombination Data Background

Recombination of atoms on RCG coated HRSI surfaces was the data used in this mechanistic modelling study. The data came from six sources: Kolodziej and Stewart (1987); Scott (1981); Stewart (oxygen data only) (1982); Willey (summer 1988) and Marinelli (1986) & (1988). Kolodziej, Scott, Stewart & Willey acquired their data from arc plasma test facilities. In Kolodziej's work, four RCG coated HRSI models, with a thickness of 3 mm., were used. The HRSI material was FRCI 20. Temperature measurements were made with Pt/PT-13% Rh thermocouples and the emissivity was reported at 0.89. Heating rates were determined by a calorimeter of known catalytic activity. To predict the recombination coefficient, the heating rate of a known catalytic reference was measured compared to the heating rate as determined by the Stephan-Boltzman equation, $Q = e\sigma T^4_w$. The calculation method used by Kolodziej and Stewart (1987), a simulation modeling and analysis of reusable thermal protection package (SMART), consisted of 3 programs: NOZZL, which calculates properties of a hot gas expanding through an arc jet nozzle; AMIR which models the inviscid bowshock in front of the blunt body; and BLIMP which models the non-equilibrium boundary layer with

FIGURE 3

Recombination Coefficients for Atomic Nitrogen
on Silica Surfaces (from Newman, 1987)

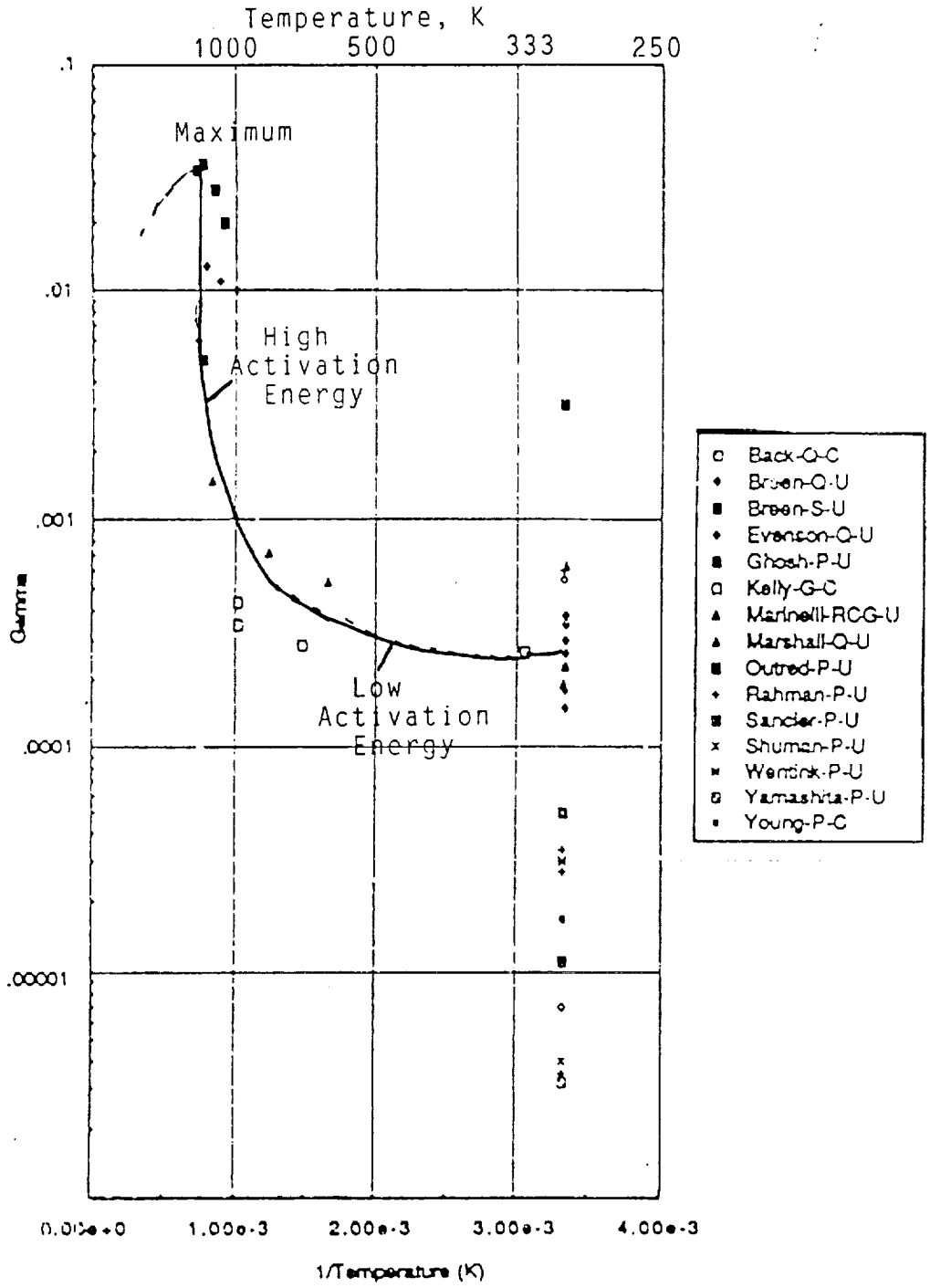

surface reaction kinetics. These programs generate curves of Q observed/Q fully catalytic (Q/Q_{FC}) as a function of gamma. Gamma is determined by the intersection of the experimental data with the predicted curves. More details are described in Kolodziej et al. 1987.

Scott and Willey also used arc plasma facilities to measure recombination coefficients. Scott (1981) used Pt/Pt-10% Rh thermocouples with the gas compositions of nitrogen and air; the enthalpies ranged from 20-37 MJ/kg and 5-31 MJ/kg for nitrogen and air respectively. The model was a flat faced RCG coated HRSI model. Willey (1988) used conditions similar to Scott with the exception that oxygen compositions were varied from 0, 11, 14 & 21 mole percents. A hemisphere model with a thermocouple located at the stagnation point of the hemisphere was used. The calculational approach used by both Scott and Willey is also described in Scott (1981). Flow field properties are determined by simple flow conservation equations for an inviscid stream tube and the flow is assumed to be a chemically frozen ideal gas. Q/Q_{FC} versus gamma curves are generated and an experimental gamma is determined from these curves. More details about the calculational routine used by Scott and Willey is available in Scott (1981).

The work of Marinelli was undertaken in a discharge flow reactor. Atom concentrations were determined by using laser-induced fluorescence and resonantly enhanced multiphoton ionization spectroscopy. Gamma was determined by solving the first order kinetic equations for oxygen concentration and was proportional to light emitted at 225 nm. More details about Marinelli experiments can be found in Marinelli, 1988.

DATA USED IN THE ANALYSIS

The mechanistic models developed in this work, were fitted to recombination coefficient data shown in Tables 1 and 2, with the first column representing the source of the data. Kolodziej and Stewart's data are from their 1987 AIAA paper. The data from Scott were presented in his 1981 paper. Two points for nitrogen from Scott were deleted from this analysis because they were off the trend shown by the bulk of his data. The data of Willey were acquired during the summer faculty fellowship program at NASA-JSC during the summer of 1988 and was reported in a summer faculty fellowship report. The datum for Marinelli (1986) for nitrogen atoms was found in a secondary source in a thesis by Newman, 1987. The second column in Tables 1 & 2 presents the temperature as read from the figures in the paper or reported. The third column reports the estimated partial pressure of the atoms at the surface of the RCG coated test article. Partial pressure was equal to the total stagnation pressure times the atomic mole fraction as reported or estimated in the various sources. The fourth column demonstrates the recombination coefficient (gamma) measured or reported. Again, gamma represents the energy transfer recombination coefficient which is a combination of the probability that atoms will combine times the fraction of energy released.

Atom concentration is related to the partial pressure by the ideal gas law: $[O] = P_O/RT$. In the reaction models which follow, the concentration of oxygen was used in place of the partial pressure of atoms.

Figures 4 and 5 show the log of gamma plotted against 1/T for all data with the exception of Marinelli's data. The data show the general trend of reaching a maximum at about 1600 K, (1000/T=0.667). Gamma decreases as temperature increases above a temperature of 1600 K (looking from right to left in the figures).

TABLE 1

Raw Data Used in the Estimation of Parameters for Various Mechanistic Models for the Recombination of Nitrogen Atoms on RCG Coated HRSI Surfaces

Source	Temp., K	Partial Pressure Nitrogen Pa	γ_N
Kolodziej & Stewart	1889	2073	0.00894
(1987)	1742	2073	0.00943
"	1686	608	0.01380
"	1603	608	0.01465
"	1467	608	0.01194
"	1422	608	0.01068
Scott (1981)	1668	1010	0.01945
"	1661	840	0.01478
"	1582	721	0.01740
"	1546	751	0.01499
"	1438	461	0.02155
"	1387	521	0.01534
"	1092	170	0.00943
"	1022	128	0.00810
"	1014	120	0.00772
"	996	92	0.00687
Willey (1988)	1536	291	0.01504
"	1524	295	0.01401
"	1506	279	0.01267
"	1496	257	0.01723
"	1493	268	0.01464
"	1490	266	0.01527
"	1460	240	0.01156
"	1412	205	0.01383
"	1411	208	0.01437
"	1402	180	0.01368
"	1350	207	0.01540
Marinelli (1986)	300	133	0.00019

TABLE 2

Raw Data Used in the Estimation of Parameters for Various Mechanistic Models for the Recombination of Oxygen Atoms on RCG Coated HRSI Surfaces

Source	Temp K	Partial Pressure Oxygen Pa	γ_O
Kolodziej & Stewart	1831	824	0.00370
(1987)	1806	412	0.01007
"	1742	412	0.01893
"	1726	824	0.00525
"	1644	235	0.01068
"	1617	412	0.00968
"	1592	235	0.03060
"	1450	235	0.01790
Scott (1981)	1647	370	0.02361
"	1493	368	0.01300
"	1419	351	0.00775
Stewart et al. (1982)	1556	451	0.01733
"	1344	406	0.01120
Willey (1988)	1557	241	0.00887
"	1552	134	0.02793
"	1540	252	0.00885
"	1527	253	0.01081
"	1522	127	0.01637
"	1518	241	0.00817
"	1501	237	0.01524
"	1497	239	0.00838
"	1486	230	0.02148
"	1479	128	0.01972
"	1458	225	0.02432
"	1456	124	0.01146
"	1449	231	0.01500
Marinelli (1988)	300	133	0.00020

FIGURE 4

Raw Data Used in the Estimation of Parameters for Various Mechanistic Models for the Recombination of Nitrogen on RCG Coated HSRI Surfaces

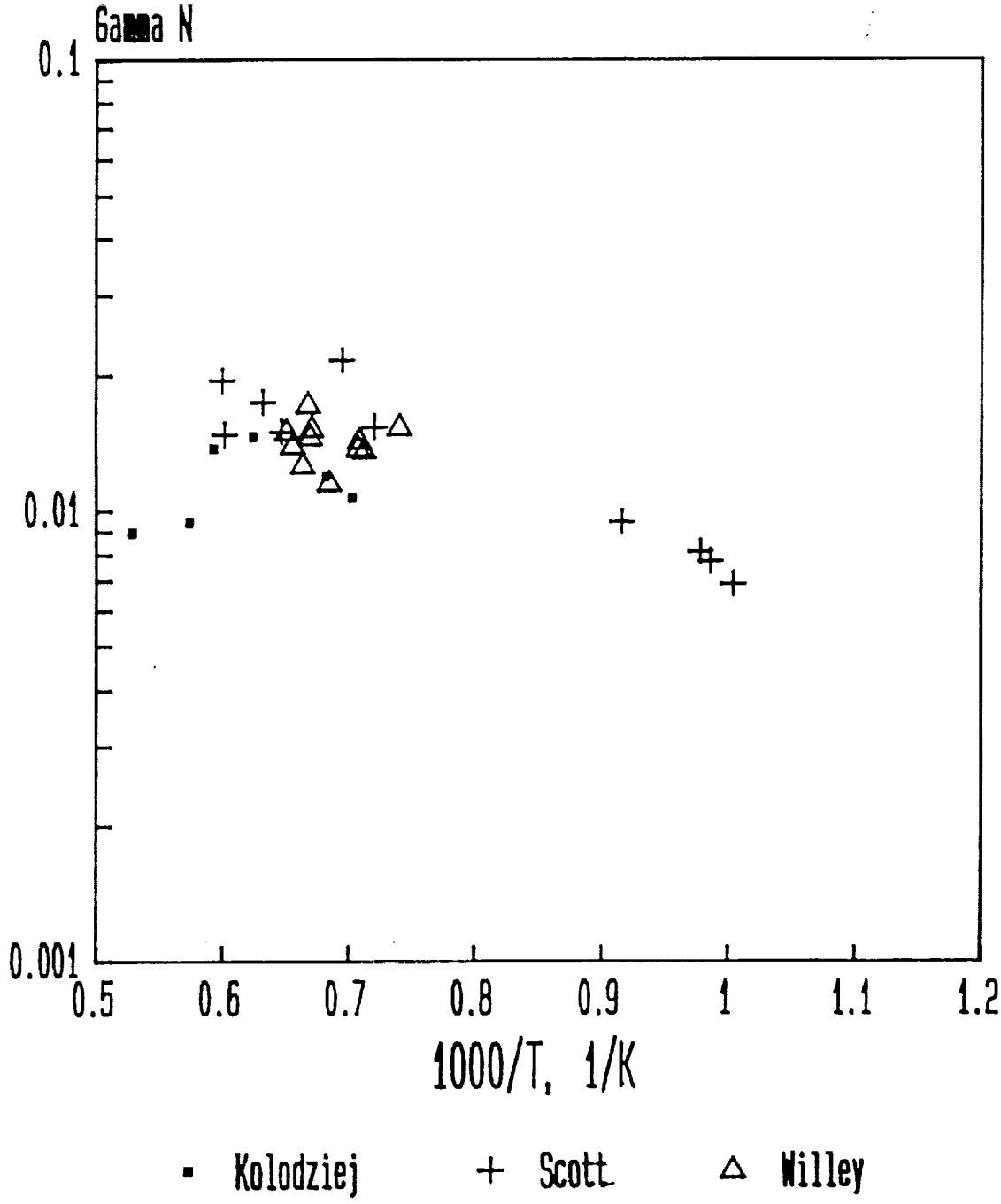

FIGURE 5

Raw Data Used in the Estimation of Parameters for Various Mechanistic Models for the Recombination of Oxygen on RCG Coated HSRI Surfaces

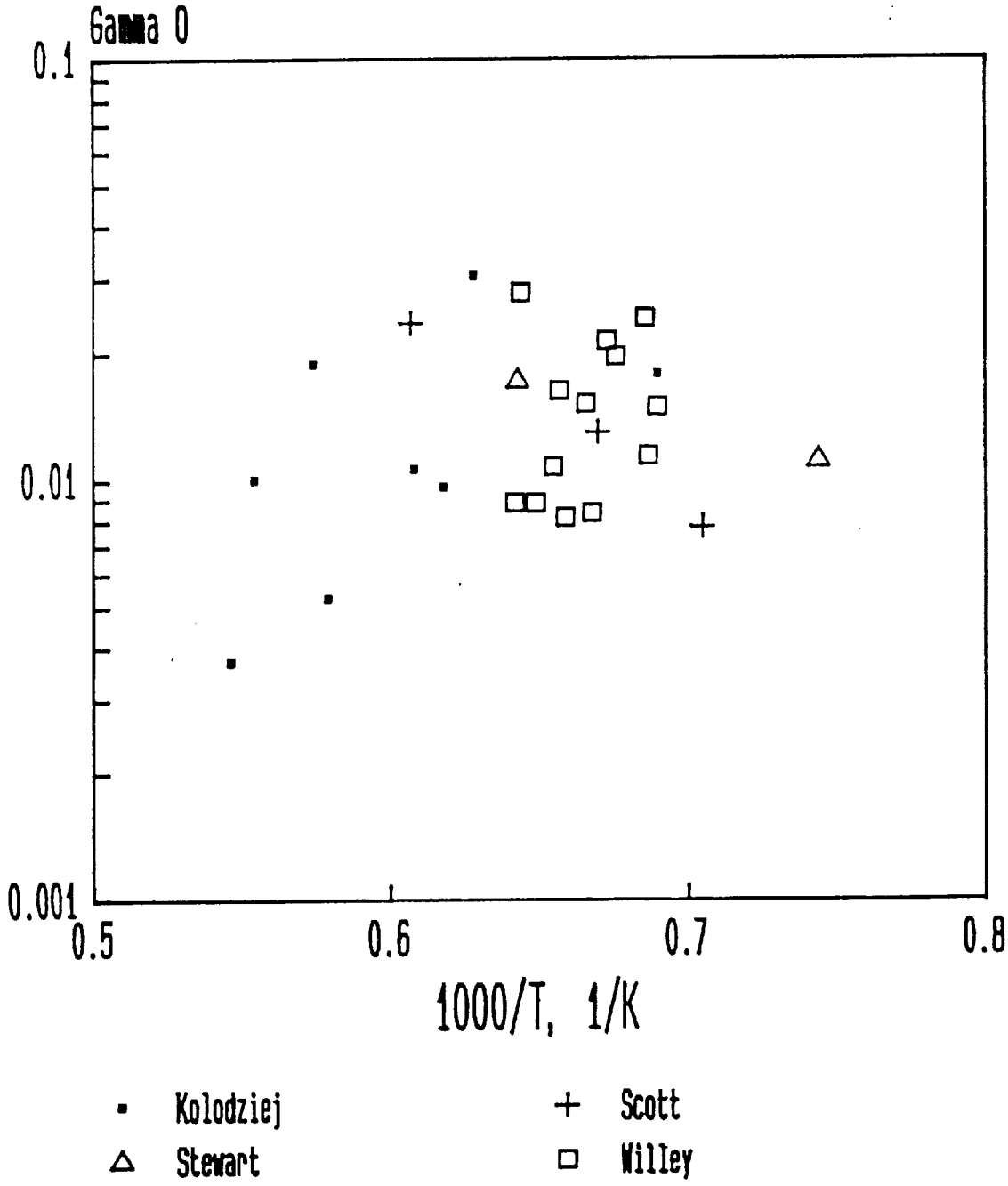

RESULTS AND DISCUSSION

Models Evaluated

Arrhenius Expression

The first model compared to the data was a simple Arrhenius expression given by:

$$\gamma_o = 2k \qquad (6)$$

where k is a function of temperature given by:

$$k = k_0 \exp(-Ea/RT) \qquad (6a)$$

and where k_0 = pre-exponential constant and

Ea = activation energy.

The value of 2 in Equation 6 reflects the stoichiometric requirement that two times the rate of molecular oxygen production equals the rate of atomic oxygen consumption. This model demonstrates that chemical reactions contain a barrier between reactants and products. This barrier is called an activation energy, or Ea. The higher the Ea the more difficult it is for reactants to go to products at low temperatures. The reaction rate is much faster at higher temperatures because higher temperatures provide the energy needed to hurdle the higher barrier. The Arrhenius model is a direct result from a standard definition of the recombination reaction being first order in oxygen atoms. The recombination rate is equal to k_w times the concentration [O].

$$\text{rate} = k_w [O] \qquad (7)$$

The recombination coefficient is defined as the ratio of the number of atoms recombined, divided by the number of atoms that strike the surface. The number of atoms which strike the surface is given by:

$$N = [O]\, c/4 = [O]\, [k_B T/2m\pi]^{1/2} \qquad (8)$$

where c is the average velocity per particle equal $[8k_B T/m\pi]^{1/2}$
and [O] is the number density of atoms, atoms/m^3.

Dividing Equation 7 by Equation 8 gives the definition of gamma in terms of the first order wall reaction coefficient, k_w.

$$\gamma = k_w(2m\pi/k_BT)^{1/2} \qquad (8a)$$

Thus, the constant k in Equation 6 is similar to the constant k_w in Equation 8a within a correction factor related to the square root of temperature. Often in chemical kinetics the square root of temperature relationships are assumed to be constant compared to the exponential factors in the reaction coefficients. Thus, the recombination coefficient for the Arrhenius expression assumes that the reaction rate at the surface is first order in oxygen concentration above the surface.[1] The Arrhenius expression predicts that when the log of gamma is plotted against 1/T, a straight line will result, whose negative slope is proportional to the activation energy and whose intercept is related to the preexponential constant. Reviewing the data in Figures 4 and 5, one sees that, indeed, a portion of the data can be described by a straight line going from right to left of a negative slope. After the temperature reaches about 1600 K, however, the Arrhenius expression fails to describe the data properly. The Arrhenius expression will be referred to as Model 0.

Recombination Models Derived from the Rideal-Eley Mechanism

The Rideal-Eley mechanism is a two-step mechanism. First an atom adsorbs onto a surface site, then the adsorbed surface atom reacts at the surface with a gas phase atom. The mechanism is as follows:

$$O + [S] \rightleftharpoons [OS] \qquad (9)$$

$$O + [OS] \text{ ---> } O_2 + [S] \qquad (10)$$

In Equation 9 , oxygen atoms are adsorbed onto reduced sites. In Equation 10, oxygen atoms near the surface combine with oxygen atoms on the surface to form O_2, plus regenerate a reduced site. Several reaction models can be found from this mechanism and

---

[1] For the recombination of nitrogen atoms, substitute nitrogen concentrations whenever oxygen concentration is discussed.

are derived in Appendix A. The simplest model from the Rideal-Eley mechanism, is to assume that Equation 9 is in pseudo-equilibrium and that Equation 10 is rate limiting. Thus, the simplest model that can be derived is as follows:

$$\gamma_o = 2k_2 K/(1 + K) \qquad (11)$$

This equation will be referred to as Model 1[2] and, when compared to Model 0, has an added term related to adsorption (K). This model predicts that at low temperatures, where adsorption dominates, gamma will be zero order in oxygen atom concentration. Equation 11 reduces to:

$$\gamma_o = 2k_2 \qquad (12)$$

The surface will be essentially bare above a certain temperature, demonstrating that as temperature increases, fewer oxygen atoms will stay on the surface. The reaction rate can then be approximated by:

$$\gamma_o = 2\ k_2\ K. \qquad (13)$$

The adsorption term, K, consists of the ratio of the forward divided by the reversed reaction rate constants in Equation 9. In general, the adsorption equilibrium constant is described by an Arrhenius behavior as given below:

$$K = Ka \exp (D/RT) \qquad (14)$$

where Ka is the preexponential constant for the equilibrium constant and D is the activation energy related to the adsorption equilibrium constant.

The equilibrium constant has a positive slope on an Arrhenius plot because adsorption is stronger at lower temperatures. As temperature increases, molecules tend to come off the surface at a faster rate than they can be absorbed. The overall results observed are dependent upon the value of D. The combined k_2K term can have either a positive or negative overall activation energy. Therefore, the behavior of the recombination coefficient at higher temperatures, can increase, stay the same, or decrease in temperature depending on the value of D compared to Ea.

---

[2] Derivations of Models 1 through 4 are in Appendix A & B.

Model 1 assumes that the concentration of oxygen atoms near the surface is constant for all conditions. Another Rideal-Eley model, Model 2, includes a concentration of oxygen atoms at the surface and is as follows:

$$\gamma_o = 2\ k_2K[O]/(1+K[O]) \qquad (15)$$

This model shows that oxygen will influence the recombination rate. At low temperatures, Model 2 reduces to:

$$\gamma_o = 2k_2 \qquad (16)$$

and at high temperatures, Model 2 reduces to:

$$\gamma_o = 2k_2K[O] \qquad (17)$$

Therefore, the recombination order will be zero order at low temperatures transitioning over to first order at high temperatures.

Model 2 effectively displays atom concentrations at the surface proving that recombination coefficients are a function of atom concentrations near the surface. Unfortunately, there is not enough data currently available to determine the true functionality of recombination coefficients with surface concentrations.

An extension of Model 2 includes a temperature correction term which appears in the derivation of the model:

$$(2m\pi/k_BT)^{1/2} \qquad (18)$$

Model 3 will essentially have the same behaviors at the low and high temperature extremes as displayed by Model 2. Model 3 is as follows:

$$\gamma_o = 2k_2\ (2m\pi/k_BT)^{1/2}K[O]/(1+K[O])^2 \qquad (19)$$

A Recombination Model Derived from the Langmuir-Hinshelwood Mechanism

In the Langmuir-Hinshelwood mechanism oxygen atoms adsorb onto the surface to form a surface oxide species. Next, two neighboring surface oxide species combine to form molecular oxygen:

$$O + [S] \rightleftharpoons [OS] \qquad (20)$$

$$[OS] + [OS] \dashrightarrow O_2 + 2\,[S] \qquad (21)$$

Equation 20 represents the adsorption of oxygen onto the surface and is similar to Equation 9 in the Rideal-Eley mechanism. Equation 21 represents the reaction of two surface oxide species to form molecular oxygen. The resultant recombination model, Model 4, is based on the assumption that Equation 20 is in pseudo-equilibrium and that Equation 21 is the rate limiting step.

$$\gamma_o = 2k_2 (2m\pi/k_BT)^{1/2}K^2[O]/(1 + K[O])^2 \qquad (22)$$

Model 4 demonstrates that at low temperatures, where adsorption dominates, the recombination coefficient is negative first order in oxygen concentration:

$$\gamma_o = 2k_2 (2m\pi/k_BT)^{1/2}/[O] \qquad (23)$$

At high temperatures, where adsorption is negligible, the recombination coefficient is first order in oxygen:

$$\gamma_o = 2\,k_2(2m\pi/k_BT)^{1/2}K^2[O] \qquad (24)$$

Thus, as temperature increases, a transition occurs from negative first order to positive first order in oxygen atom concentration at the surface. The available data, however, are limited and more testing is suggested to verify the possibility of this mechanism. Once again, the constant, k_2, and equilibrium constant, K, follow Arrhenius relationships as discussed in the Rideal-Eley mechanism.

Seward Model

The Seward model was developed in his 1985 thesis and is based around the Rideal-Eley mechanism using first principle kinetics to describe the adsorption, desorption, and reaction rate steps separately. This model, Model 5, consists of eight parameters:

$$\gamma_o = 2\ P\ N_o\ So\ \exp(-Ea/RT)/(SoN_o + \delta + PN_o \exp(-Ea/RT)) \qquad (25)$$

The term P represents the steric factor and is related to the ability of oxygen atoms to absorb. Seward allowed this factor as a function of temperature, up to a certain constant. The So term is related to the sticking coefficient and predicts the probability that an atom will adhere once it strikes the surface. Seward also demonstrated this constant as a function of temperature. The exponential term in the numerator is related to the forward reaction rate of step 2 in the Rideal-Eley mechanism. The term delta in Seward's equation is related to the desorption step in Equation 9 of the Rideal-Eley mechanism and consists of an activation energy and several constants related to the number of surface sites. Further explanation of the Seward model is presented in Appendix A.

Model 5 has three characteristic temperature ranges: at low temperatures adsorption of atoms onto the surface dominates, and reduces to:

$$\gamma_o = 2P \exp(-Ea/RT) \qquad (26)$$

As temperature increases, the forward reaction rate of step 2 increases. Thus, the exponential term dominates in the denominator and the numerator:

$$\gamma_o = 2\ So \qquad (27)$$

Finally, at high temperatures, the desorption of oxygen atoms dominates and the following approximation results:

$$\gamma_o = 2\ P\ N_o So \exp(-Ea/RT)/\delta \qquad (28)$$

Model 5 predicts zero reaction order at low and medium temperatures in oxygen atom concentration; at higher temperatures, the model becomes first order in oxygen atom concentrations. The steric factor and the sticking coefficient in Model 5 are allowed to be a function of temperatures, and therefore, at lower temperatures the model concaves upwards. An attractive feature of this model is that it predicts low activation energy for

recombination at low temperatures, changing to a higher activation energy at moderate temperatures. The difficulty in the application of Model 5 is the determination of the eight parameters (there are too many parameters for the data that is currently available).

Willey Empirical Model

A six parameter empirical model, Model 6, is compared to the data available:

$$\gamma_o = 2(k_2 + k_3)K/(1+K) \qquad (29)$$

This model can be thought of as the combination of two mechanistic steps, the rate being determined by the fastest of the two steps, with each step dependent upon activation energy. In this work, the rate constant k_3 dominates at low temperatures. At moderate temperatures the recombination coefficient is described by k_2 and at high temperatures the recombination coefficient is described by $2k_2K$

Model 6 can predict a concave upwards curve at low temperatures for the recombination coefficient as a function of 1/T. For the recombination of nitrogen atoms on silica, as shown in Figure 3, the activation energy for the recombination coefficient increases as temperature increases. Finally, at high temperatures, where desorption dominates, the overall activation energy goes from negative to positive and therefore the recombination coefficient declines as temperature further increases. Model 6's parameters can be adjusted to reflect the behavior shown in Figure 3. Information concerning concentration dependence on recombination coefficients is lacking and, therefore, a concentration term is not included in Model 6. A summary of mechanistic models evaluated in this report is shown in Table 3.

TABLE 3

Summary Mechanistic Models Evaluated
for Recombination Coefficients for N and O Atoms.

Model #	Name	Model
0	Arrhenius	$\gamma_o = 2\ k_2$
1	Rideal-Eley without Concentration Terms	$\gamma_o = \dfrac{2\ k_2\ K}{(1 + K)}$
2	Rideal-Eley	$\gamma_o = \dfrac{2\ k_2\ K\ [O]}{(1 + K\ [O])}$
3	Rideal-Eley with a Temperature Correction Factor	$\gamma_o = \dfrac{2\ k_2\ (2m\pi/k_BT)^{1/2}\ K\ [O]}{(+ K\ [O])}$
4	Langmuir-Hinshelwood	$\gamma_o = \dfrac{2\ k_2\ (2m\pi/k_BT)^{1/2}\ K^2\ [O]}{(1 + K\ [O])^2}$
5	Seward	$\gamma_o = \dfrac{2\ P\ N_o\ So\ \exp(-Ea/RT)}{(SoN_o + S + P\ N_o\ \exp(-Ea/RT))}$
6	Willey	$\gamma_o = \dfrac{2\ K\ (k_2 + k_3)}{(1 + K)}$

Notes:

k_2 is a function of temperature given by: $k_2 = k_{20} \exp(-Ea/RT)$

k_3 is a function of temperature given by: $k_3 = k_{30} \exp(-Ea_3/RT)$

K is a function of temperature given by: $K = Ka \exp(D/RT)$

[O] is the concentration of oxygen atoms at the surface in atoms/m^3; for nitrogen substitute [N] for [O] in any of the above models

The value of R in these models is 0.0083144 kJ/g mole/K

Determination of Constants

For the models presented above, the parameters were determined by non-linear least squares on the log of gamma. The log of gamma was chosen because it would give equal weight to lower gammas at lower temperatures. Therefore, the parameters chosen were those which minimized the sum of squares of error (SSE) defined as: $\Sigma[(\log \gamma_{(i)\,obs}) - \log (\gamma_{(i)\,pred})]^2$. All plots presented are log gamma versus 1/T. Model 0 was simple to evaluate by linear regression on log gamma versus 1/T because the slope is proportional to the activation energy and the intercept is equal to 1/2 of k_2. The parameters for Models 1-4 were determined by using a non-linear least squares routine, BMDP PAR, for derivative free non-linear models. Models 1-4, it was discovered, have poorly conditioned surfaces and the parameter's joint confidence regions have very narrow but broad cigar shape surfaces (Draper & Smith, 1986). To provide assistance in determination of constants by non-linear squares, the models were reparameterized as suggested in Draper & Smith by shifting the rate constant k_2 by the factor of 1000/T-3.333. The preexponential constant therefore, was centered at 300 K with the determined activation energy being 1/1000 of the true activation energy. For K, 1/T was shifted to 1000/T-0.54, centering Ka at 1852 K. This resulted in faster converging least squares routines. A limit was also placed on the maximum value of D, the desorption activation energy, of 574 kJ/mole, preventing arithmetic overflows during the determination of the constants.

The constants for Model 5 were determined using LOTUS 123 with a single parameter perturbation interactive approach. Each parameter was individually varied to determine the direction of the sum of squares of error (SSE) on log gamma. Then, depending upon which parameter reduced the SSE the most, that parameter was corrected and new parameters were found. The parameters for Model 6 were determined by choosing activation energy for the low temperature reaction coefficient, k_3. The values used were 640 cal/mole or 2.67 kJ/mole for nitrogen, and 1,000 cal/mole or 4.19 kJ/mole for oxygen atoms. These numbers are based on data for recombination of atoms on silica as

presented in Newman's and Seward's theses (1987, 1985). The remaining parameters in that model were determined by non-linear least squares.

Application of Models

Table 4 presents the overall summary. The models are compared to the recombination data for the recombination of nitrogen and oxygen atoms on RCG coated HRSI materials. The best fits were achieved by Model 1, as demonstrated by the low SSE in Table 4 for both cases. Willey's Model 6 also closely resembles the data, giving a slightly lower SSE for nitrogen and slightly higher SSE for oxygen. Figures 6 through 12 and Figures 13 through 19 (beginning on page 32) show a graphical representation for various models compared to the data used. Figures 6 through 12 illustrate recombination of nitrogen atoms on RCG coated HRSI surfaces and Figures 13 through 19 illustrate recombination of oxygen atoms on RCG coated HRSI surfaces. This arrangement portrays the relation of each model to the data for recombination of nitrogen and oxygen atoms. Figures 20 through 23 are residual plots for the various models evaluated: Figure 20 for the recombination coefficient for nitrogen as a function of 1/T; Figure 21 for the nitrogen recombination coefficient versus partial pressure of nitrogen atoms; Figure 22 for the various recombination models for oxygen atoms as a function of 1/T; and Figure 23 for the various recombination models for oxygen atoms as a function of the partial pressure of oxygen atoms. These residual plots are helpful in determining the sufficiency and insufficiency of the various models used by noting trends and making corrections as needed.

The results from Model 0 are shown in Figures 6 and 13 for nitrogen and oxygen recombination coefficients respectively. Model 0 predicts a straight line on an Arrhenius type plot with deviations occurring at higher temperatures. Figures 20-A for nitrogen and 22-A for oxygen show the lack of fit at low 1/T values where the actual data falls below

TABLE 4

Residual Sum of Squares Summary for Various Recombination Coefficient Models

Model #	Name	S.S.E.[1] for Nitrogen	S.S.E. for Oxygen
0	Arrhenius	0.254	1.357
1	Rideal-Eley without Concentration Terms	0.138	0.938
2	Rideal-Eley	0.150	1.044
3	Rideal-Eley with Temperature Correction Factor	0.167	1.044
4	Langmuir-Hinshelwood	2.259	1.019
5	Seward's	0.206	1.134
6	Willey	0.136	1.021

[1] Sum of Squares of Errors on log gamma

that predicted. It is necessary to create models that would better predict recombination coefficients at higher temperatures.

The results of Model 1 are shown in Figures 7 and 14 for nitrogen and oxygen atom recombination coefficients. These figures show a maximum in recombination coefficient as temperature increases; the maximum occurs at about 1600 K with a maximum predicted recombination coefficient of 0.013 for nitrogen and of 0.014 for oxygen. The residual plots confirm the suitability of this model. These plots are shown in Figures 20-B, 21-B, 22-B and 23-B. Figure 23-B shows a slight negative trend, indicating that the model is deficient in a concentration term.

The results for Model 2 are shown in Figures 8 and 15 for nitrogen and oxygen atom recombination coefficients, demonstrating the influence of atom concentration (atom partial pressure) in terms of the Rideal-Eley mechanism. Figure 8 shows predicted recombination coefficients for partial pressure of nitrogen atoms at the surface of 100, 500 and 2,000 Pa. The recombination coefficient has a first-order functionality on partial pressure (concentration) at higher temperatures; at low temperatures, the three pressure predictions combine into a single curve on the right hand side of Figures 8 and 15 because the partial pressure functionality is zero-order. Thus the Rideal-Eley model predicts a zero-order concentration functionality at lower temperatures.

Model 2 shows wider residual plots (Figures 20-C, 21-C, 22-C, 23-C) compared to Model 1, and a negative trend in pressure appears for oxygen atoms (Figure 23-C). Nitrogen residuals also show a slight negative trend in terms of pressure (Figure 21-C). These residual plots, as a function of pressure, indicate that the model should be at least one order less in pressure.

In Model 3, the addition of a temperature concentration term $(2M\pi/k_BT)^{1/2}$ does not enhance the fit of data. Figures 9 and 16 show very similar results to Figures 8 and 15,

however a slight concave downward appearance occurs in the curves for the low temperature region between 300 and 1000 K. This appearance occurs because of the $T^{1/2}$ in the numerator of the Model 3. Again, the recombination coefficient is independent of concentration up to about 1500 K, after which it becomes first-order in concentration. The first-order influence can be seen in Figure 9 where the curves separate at higher temperatures for the partial pressures of nitrogen of 100, 500, and 2000 Pa. A further complication occurs in the determination of the parameters for this model; the upper boundary of the adsorption activation energy of 574 kJ/mole was reached for both oxygen and nitrogen. As further supporting data becomes available, the maximum can be increased.

Model 4, the Langmuir-Hinshelwood Model, shows a poor fit for the nitrogen data (Figure 10) and a good fit for the oxygen data (Figure 17). In determining the parameters for nitrogen atom recombination in Model 4, boundaries were reached in which an arithmetic overflow occurred during the computational steps. Therefore, the parameters chosen are at the boundary for Ka and for D. The model essentially looks like a negative first-order for nitrogen atoms throughout the whole region. In Figure 17, the recombination rate is higher for lower partial pressures for oxygen atoms with the curves at 100, 400 and 800 Pa falling beneath each other sequentially. The data, which had different pressures depending upon the researcher, were well described by Model 4 considering the wide range of variables studied. These results suggest that measurements be taken in the 500 to 1000 K range for oxygen recombination, varying the oxygen concentration at two or three levels. For instance, experiments could be run in the current arc jet facilities studying oxygen concentrations of 5%, 10%, and 21%, which would vary the concentration of atoms at the surface. The Langmuir-Hinshelwood model explains the observation of higher recombination rates at lower pressures; a maximum in the recombination coefficient is reached in this model as a function of concentration because the reaction requires two neighboring sites. This maximum occurs when the surface is about half covered with adsorbed atoms, when half of the sites are empty and half of the sites are covered. When

the surface is bare no reaction occurs, because nothing is on the surface. On the other extreme, at higher pressures, where the surface is covered, atoms which are near the surface cannot adsorb but must wait until two atoms combine on the surface and desorb; therefore, the maximum occurs when the surface is half covered. Although good data is unavailable to confirm this model, experiments need to be conducted at temperature regions between 500 and 1000 K with the partial pressure of oxygen purposely varied in order to determine an influence of recombination coefficient as a function of pressure. These experiments would provide the evidence required to support a Langmuir-Hinshelwood recombination model.

The results for Model 5 are shown in Figures 11 and 18 for nitrogen and oxygen atom recombination coefficients respectively. In Figure 11, as temperature increases, the model is concave upward. Seward's model achieves this by changing the parameters P and S, and a maximum gamma is reached at about 1600 K. At temperatures above 1,600 K, gamma decreases and the functionality is first-order in the partial pressure of atom concentration. At high temperatures, Model 5 is very similar to the Rideal-Eley mechanism. The residual plots for Model 5, Figures 20-F, 21-F, 22-F, and 23-F, show good scatter of the data points around zero.

Model 6, the empirical model, is shown in Figures 12 and 19 for nitrogen and oxygen atom recombination coefficients respectively. This particular model has no concentration term, but does predict that the recombination coefficient will increase to a maximum as temperature increases and then decrease as temperature increases further. Model 6 also demonstrates concave upward behavior in the low temperature region. This is based on data from atom recombination on silica type surfaces which are very similar to RCG coated surfaces. These results suggest that the activation energy at low temperature is lower compared to activation energy at higher temperatures. Thus, the activation energy changes with temperature. The observed activation energy is the combination of two parallel reaction's activation energies; one reaction going faster at low temperature and

the other speeding up at high temperature. The activation energy chosen for the low temperature reaction was based on values reported by Newman (1987) and Seward (1985) for nitrogen and oxygen atoms respectively. They reported the activation energy to be 640 cal/mole for nitrogen atom recombination, and 1000 cal/mole for oxygen atom recombination on silica surfaces at low temperatures. The residual plots for Model 6, shown in Figures 20-G, 21-G, 22-G, and 23-G, demonstrate a good fit in all cases, except for a slight negative trend in terms of pressure for oxygen.

Table 5 presents the parameter estimates for the various recombination models evaluated. Column 1 represents the model number which corresponds to the model number in Table 3, columns 2 and 3 present the parameter name and its units. Rate constants and equilibrium constants are composed of two terms: a preexponential constant and an activation energy. Columns 4 and 5 are the parameter values which give the minimum sum of squares of errors for the comparison of each model to the data. The confidence limits for the parameters are not presented because of the poorly conditioned non-linear surfaces encountered with these models.

In summary, a model independent of concentration describes the available data. The recombination model can be one of two versions, depending upon future results of low temperature recombination experiments: if data falls in the lower regions at 500 K (Figures 12 and 19) Model 6 should be used; if data falls upon a straight line between 300 and 1000 K (Figures 7 and 14) Model 1 is more appropriate. If, in a further work, a concentration functionality is found important, then data should be compared to Models 2 to 5 (Figures 8 to 11, Figures 15 to 18).

TABLE 5.

Parameter Estimates for Various Recombination Models Evaluated

Model #	Parameter Name	Parameter Units	Value for Nitrogen	Value for Oxygen
0	k_{20}	Unitless	0.019879	0.017057
	Ea	kJ/mole	13.247	12.585
1	k_{20}	Unitless	0.021953	0.020155
	Ea	kJ/mole	13.580	13.235
	Ka	Unitless	1.0647E-07	5.7376E-16
	D	kJ/mole	249.318	520.880
2	k_{20}	unitless	0.021660	0.019763
	Ea	kJ/mole	13.545	13.186
	Ka	m^3/atom	1.2309E-33	8.6919E-40
	D	kJ/mole	359.890	574.340
3	k_{20}	m/sec	9.64640	8.54460
	Ea	kJ/mole	15.971	15.705
	Ka	m^3/atom	9.1630E-35	9.7166E-40
	D	kJ/mole	404.250	574.340

TABLE 5. Continued

Model #	Parameter Name	Parameter Units	Value for Nitrogen	Value for Oxygen
4	k_{20}	atom/m^2/sec	1.5283E+23	8.1484E+22
	Ea	kJ/mole	14.209	12.676
	Ka	m^3/atom	1.9649E-19	1.8112E-38
	D	kJ/mole	574.340	574.340
5	D	kJ/mole	353.500	339.000
	Ea	kJ/mole	4.593	4.185
	C_a	atoms/m^2	1.10E+20	7.94E+19
	P_0	unitless	2.25E-04	1.79E-04
	P_2	1/K	3.12E-03	2.92E-03
	Max P	unitless	0.04	0.10
	S_{01}	unitless	3.16E-01	5.01E-01
	S_1	1/K	-2.00E-03	-2.00E-03
6	k_{20}	unitless	3.9885E-02	7.4805E-01
	Ea_2	kJ/mole	20.409	58.861
	k_{30}	unitless	2.4275E-04	4.2845E-04
	Ea_3	kJ/mole	2.677	4.189
	Ka	unitless	2.8098E-08	1.4158E-14
	D	kJ/mole	262.921	458.036

FIGURE 6

Comparison of Model 0 with the Recombination Coefficients
for Nitrogen Atoms on RCG coated HRSI Materials

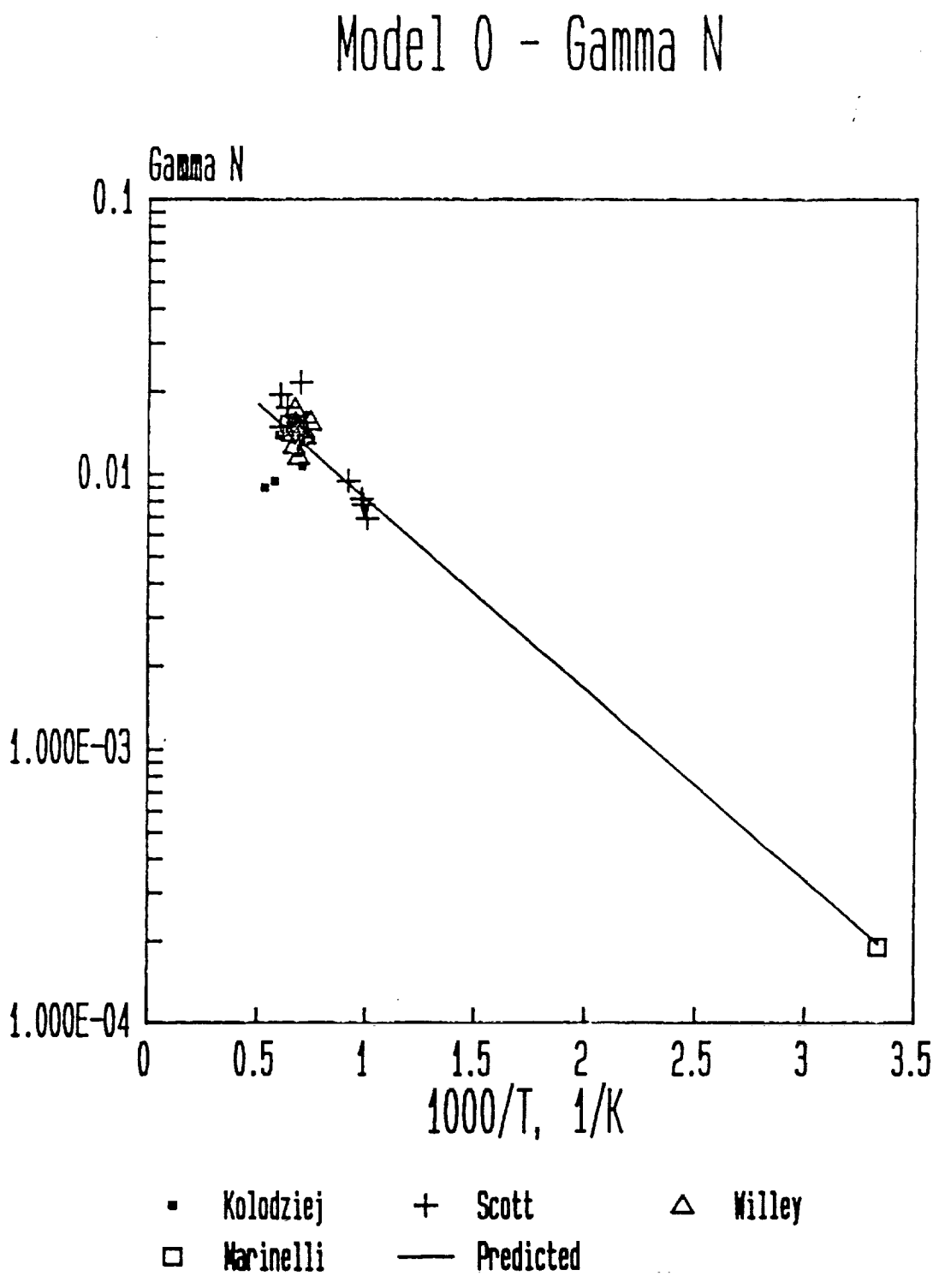

FIGURE 7

Comparison of Model 1 with the Recombination Coefficients
for Nitrogen Atoms on RCG Coated HRSI Materials

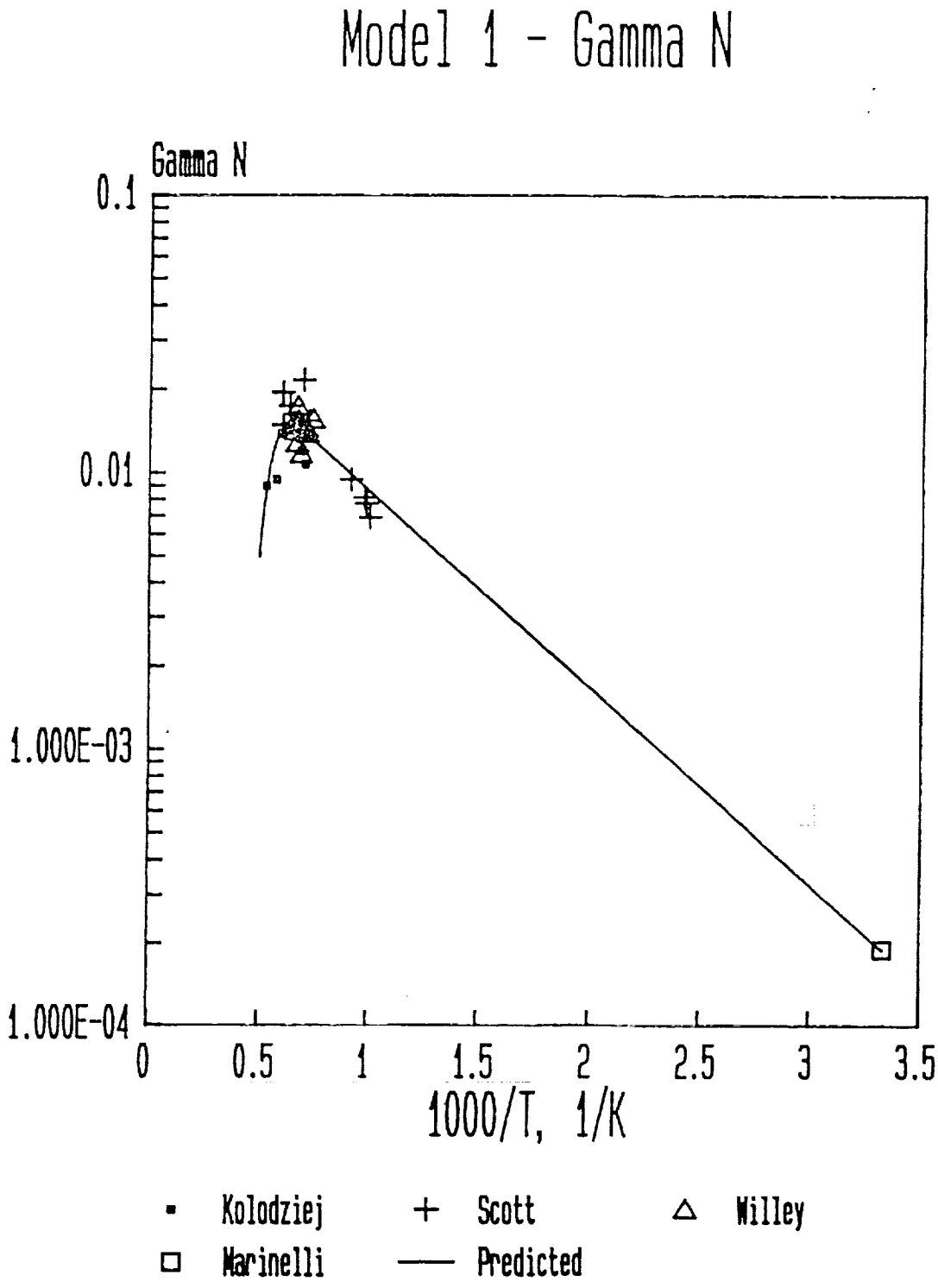

FIGURE 8

Comparison of Model 2 with the Recombination Coefficients
for Nitrogen Atoms on RCG coated HRSI Materials

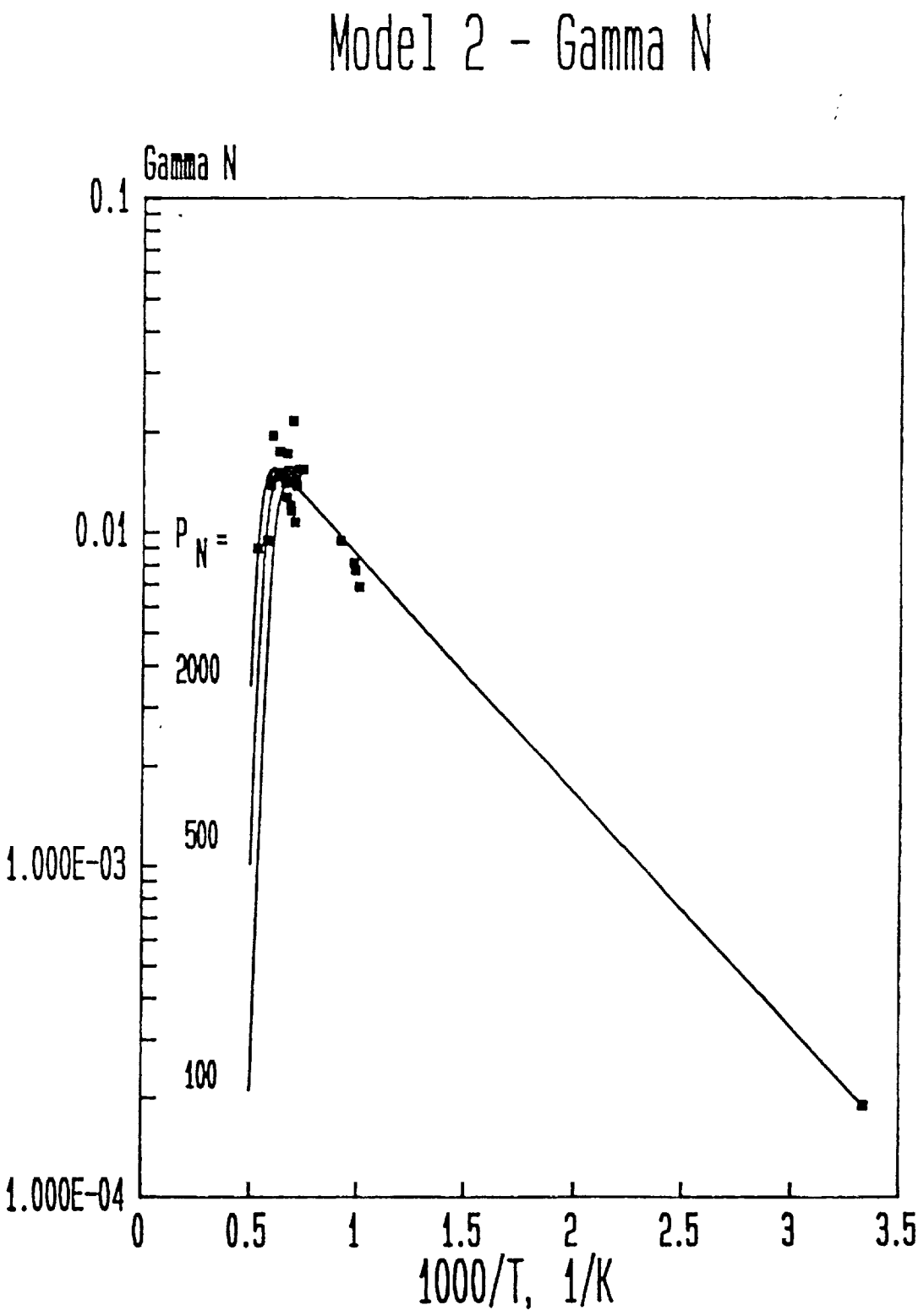

FIGURE 9

Comparison of Model 3 with the Recombination Coefficients
for Nitrogen Atoms on RCG Coated HRSI Materials

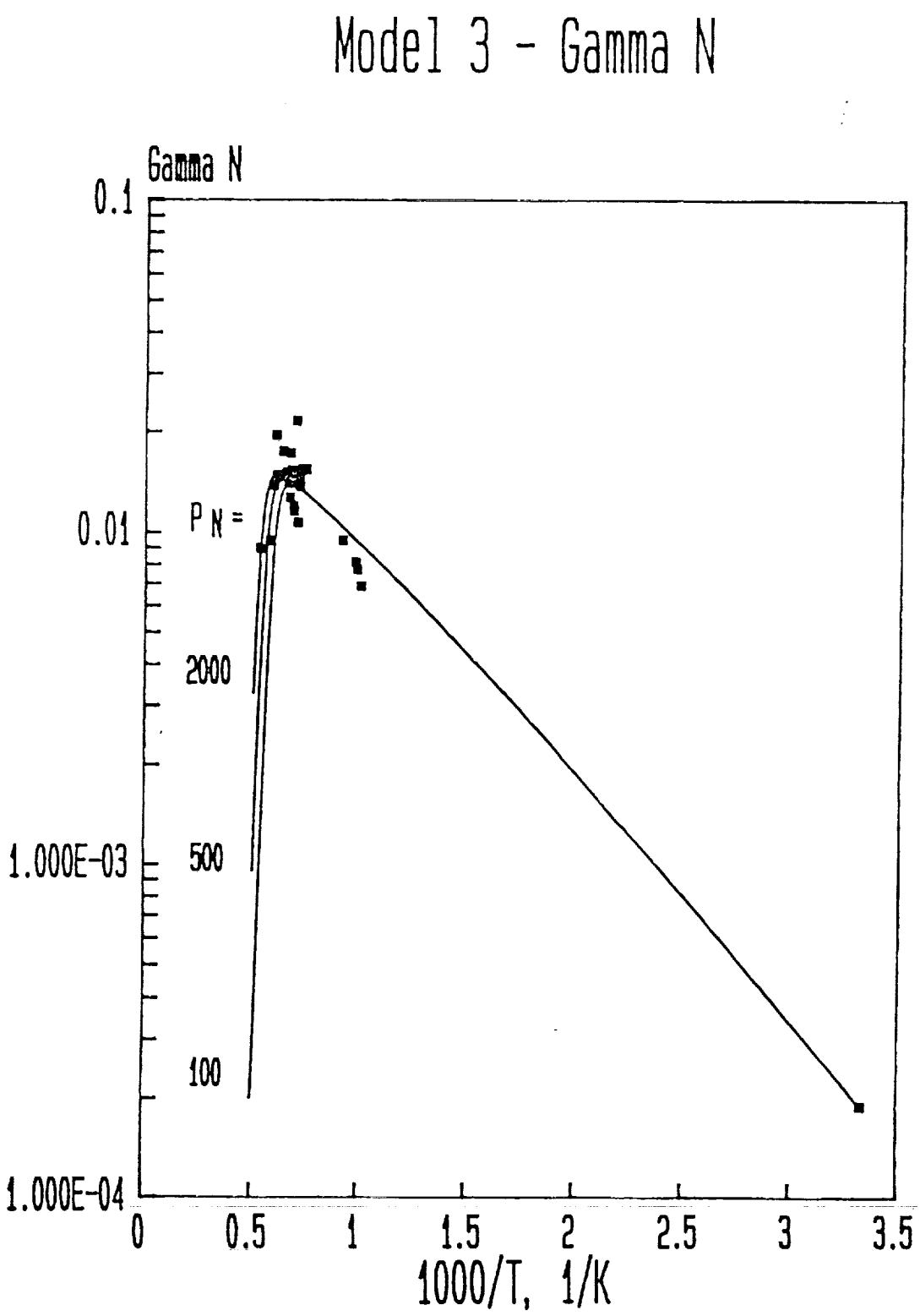

FIGURE 10

Comparison of Model 4 with the Recombination Coefficients for Nitrogen Atoms on RCG Coated HRSI Materials

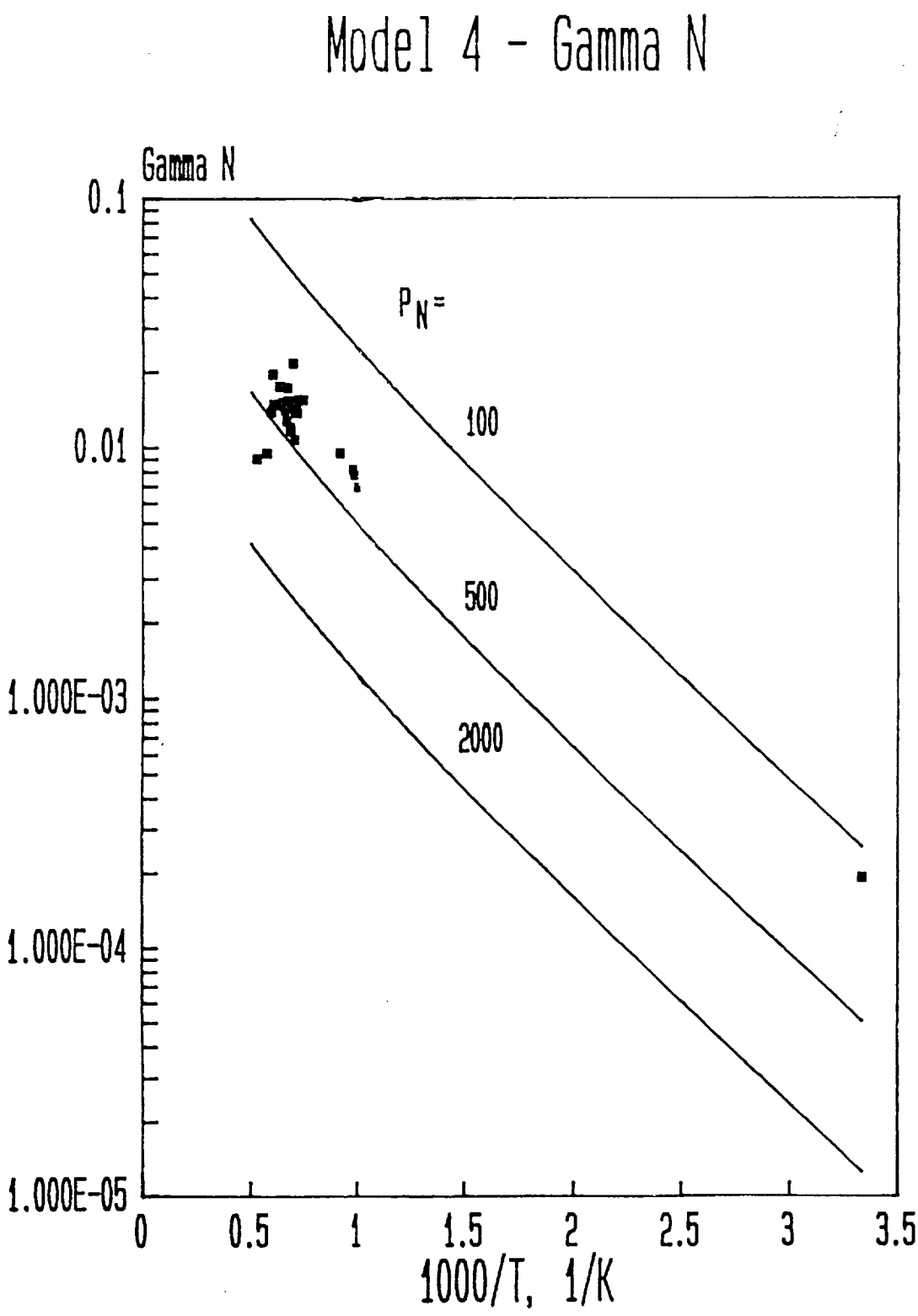

FIGURE 11

Comparison of Model 5 with the Recombination Coefficients
for Nitrogen Atoms on RCG Coated HRSI Materials

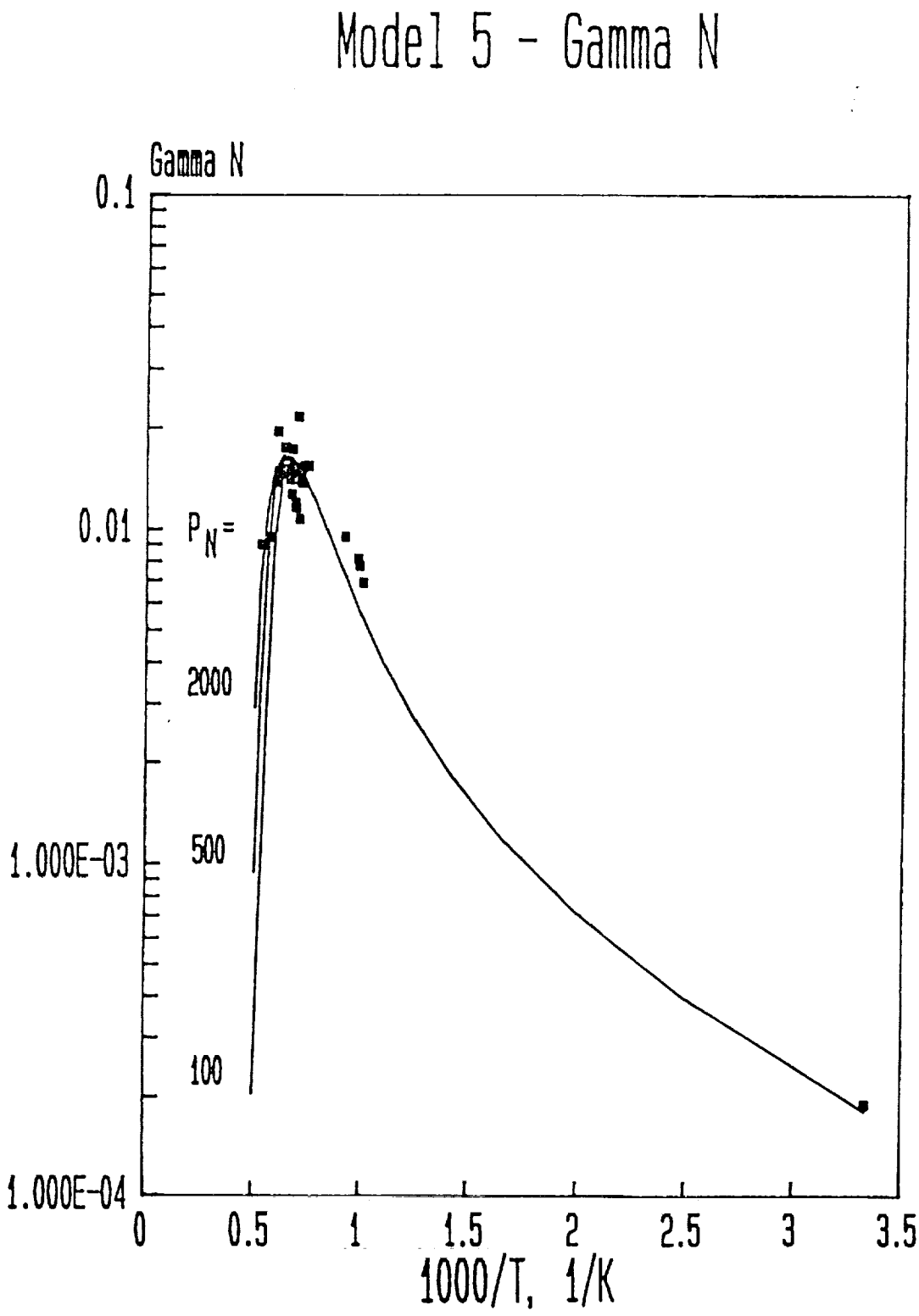

FIGURE 12

Comparison of Model 6 with the Recombination Coefficients
for Nitrogen Atoms on RCG Coated HRSI Materials

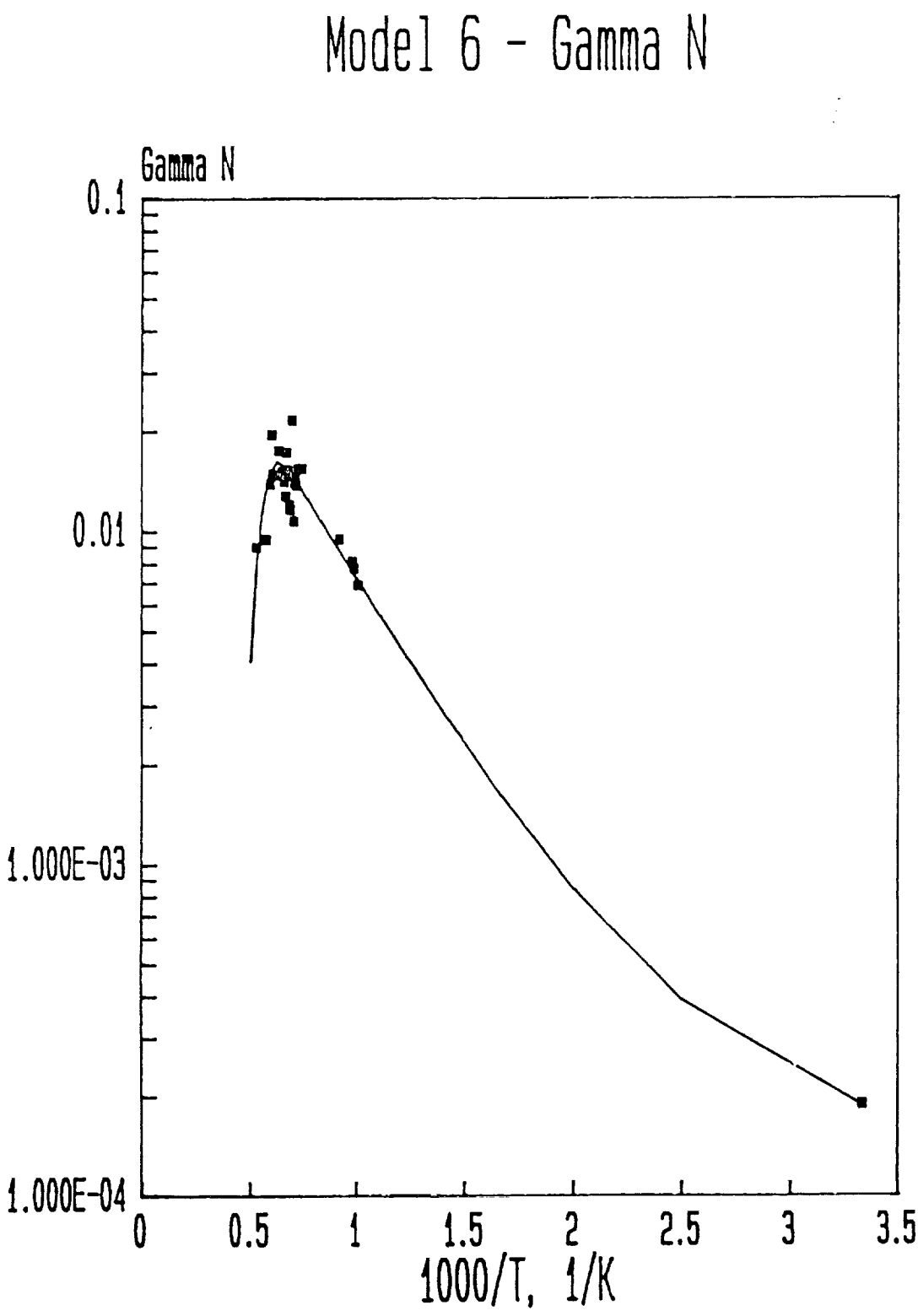

FIGURE 13

Comparison of Model 0 with the Recombination Coefficient
for Oxygen Atoms on RCG Coated HRSI Materials

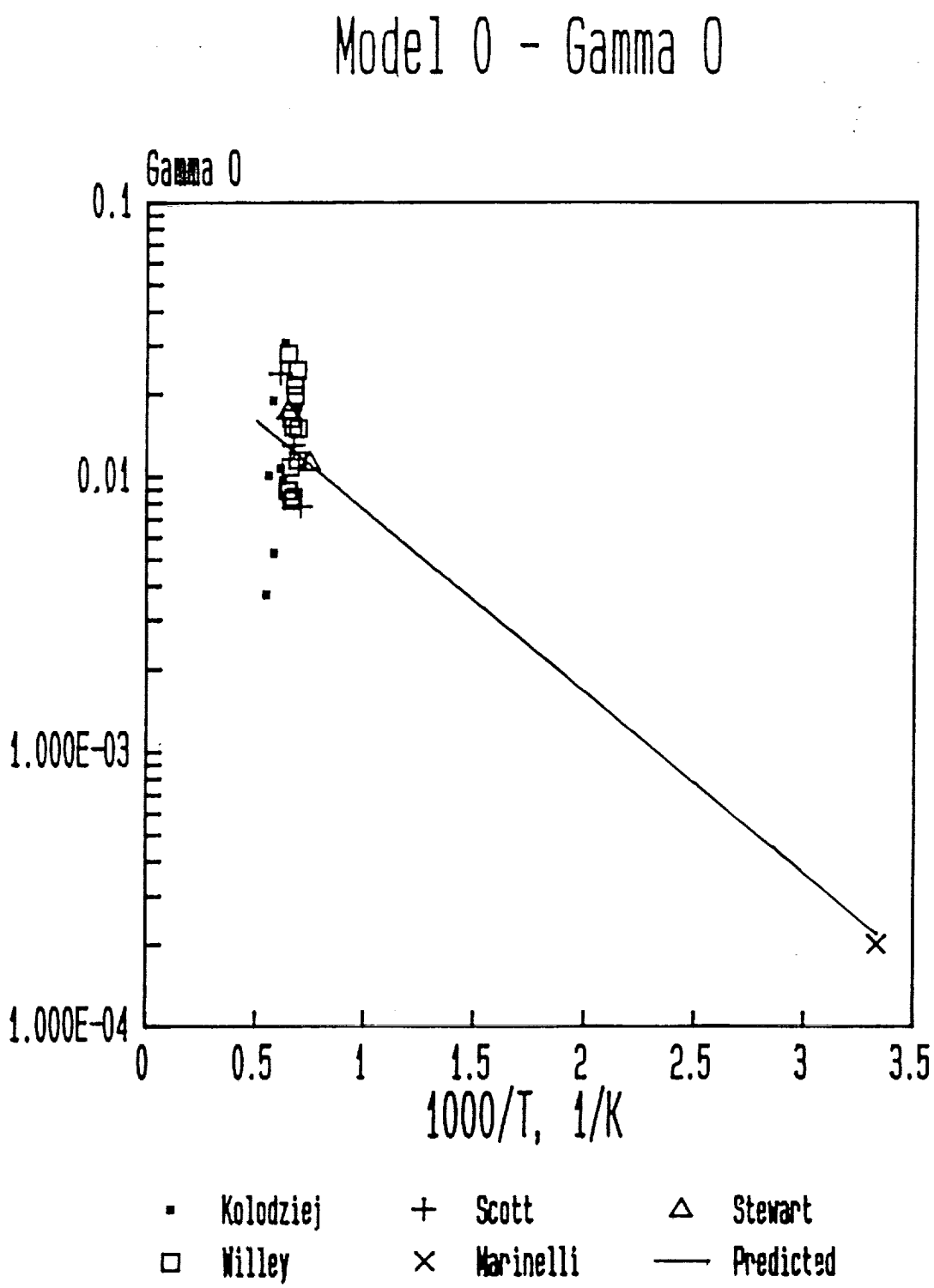

FIGURE 14

Comparison of Model 1 with the Recombination Coefficient for Oxygen Atoms on RCG Coated HRSI Materials

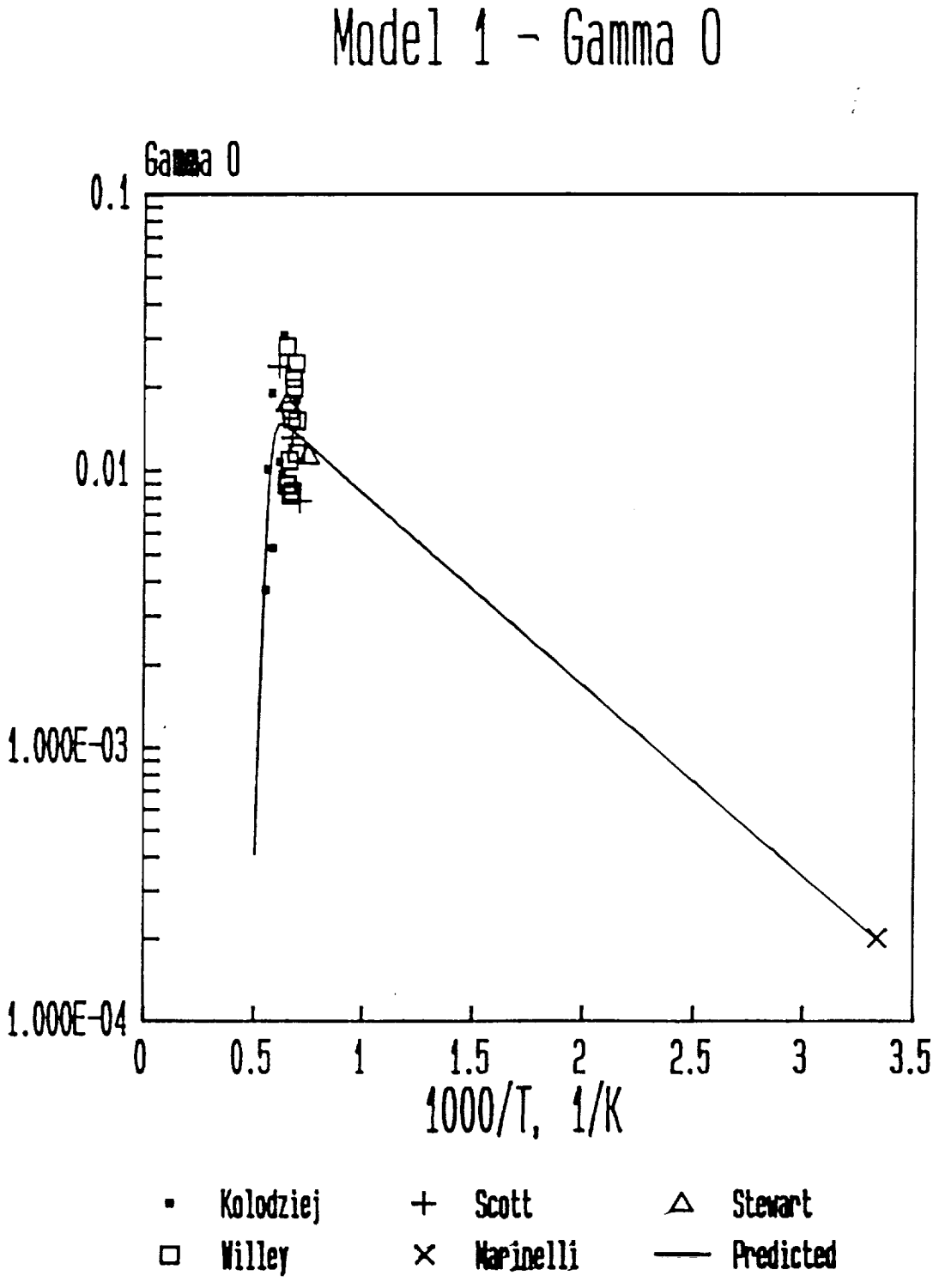

FIGURE 15

Comparison of Model 2 with the Recombination Coefficient for Oxygen Atoms on RCG Coated HRSI Materials

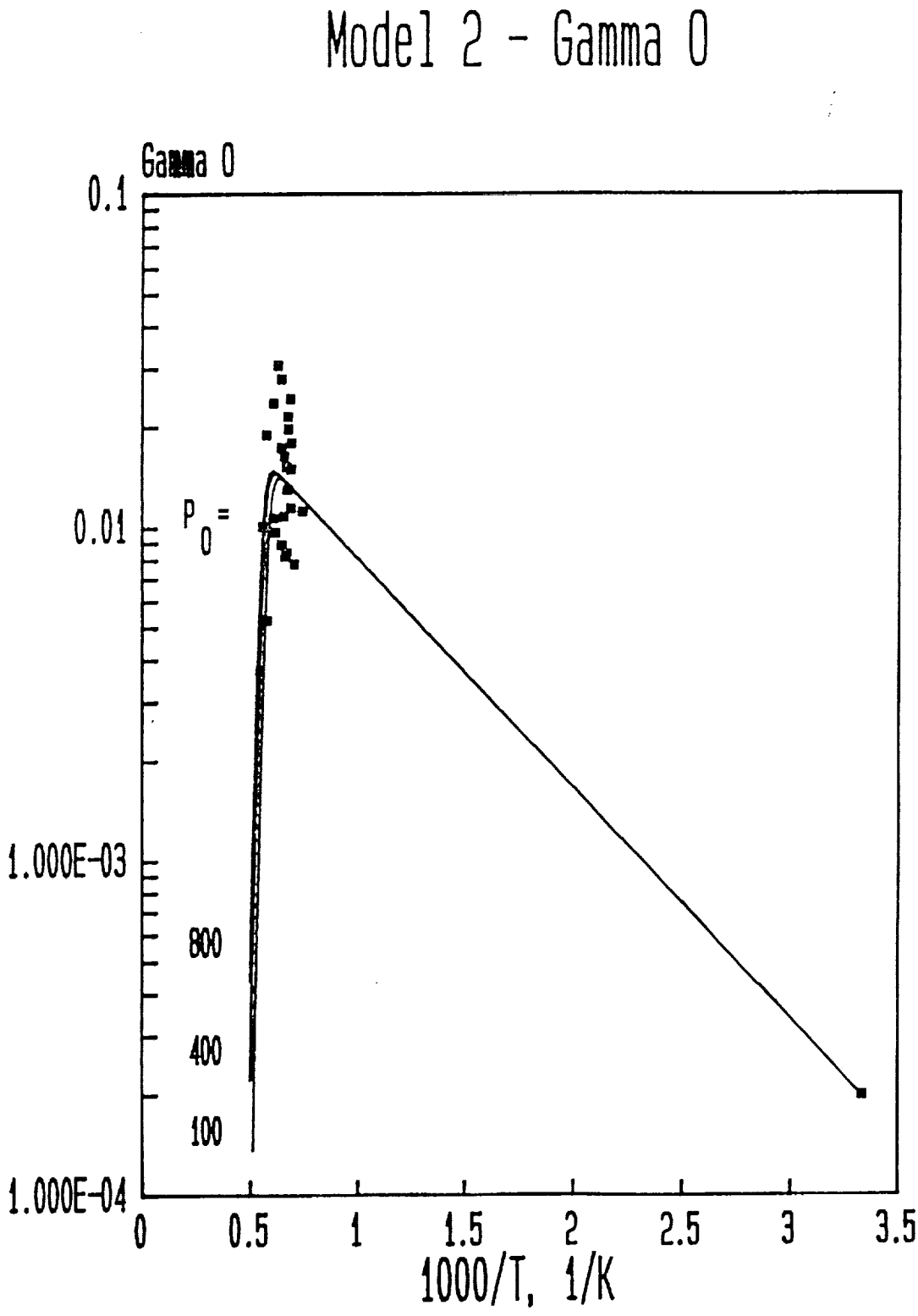

FIGURE 16

Comparison of Model 3 with the Recombination Coefficient for Oxygen Atoms on RCG Coated HRSI Materials

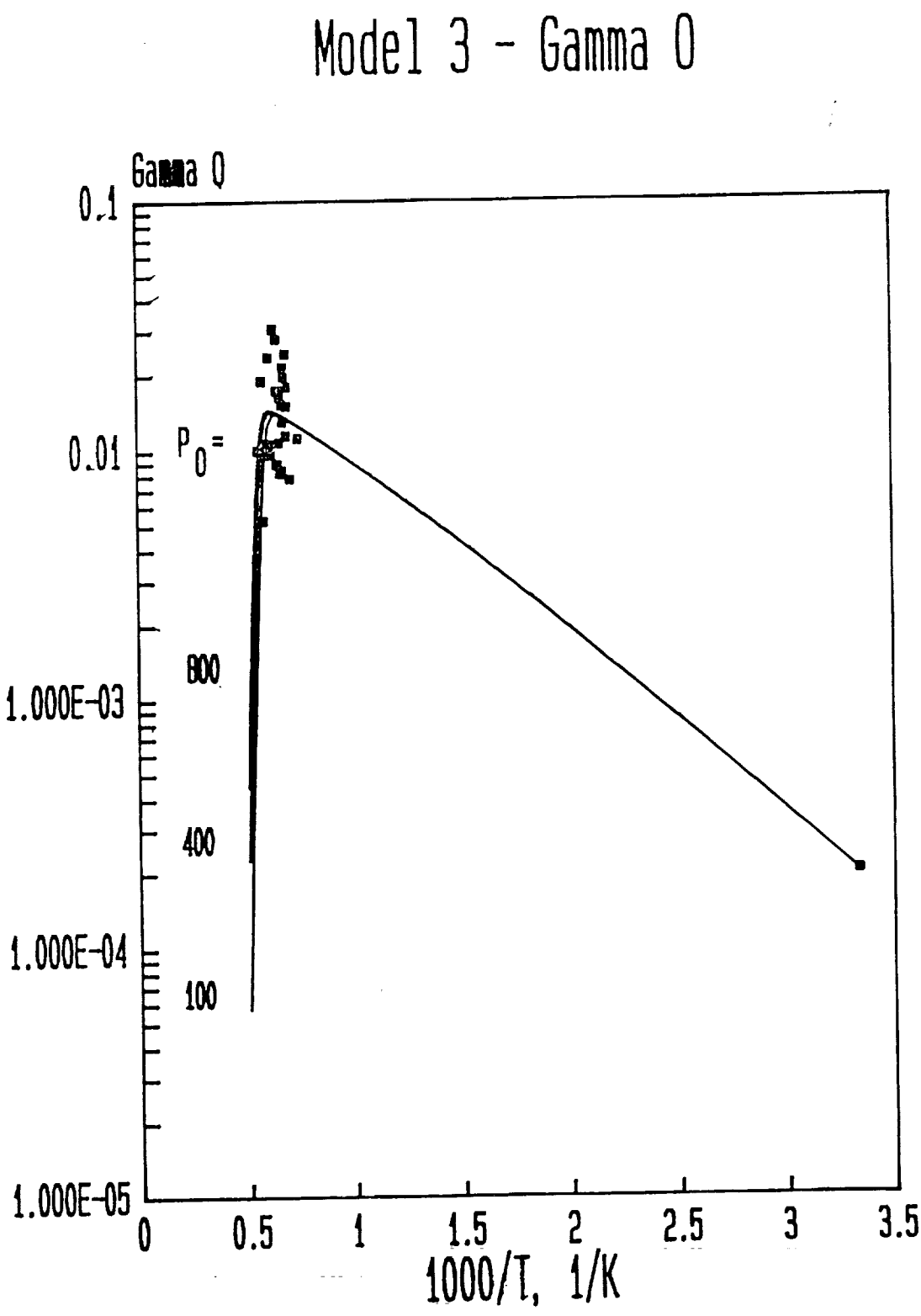

FIGURE 17

Comparison of Model 4 with the Recombination Coefficient
for Oxygen Atoms on RCG Coated HRSI Materials

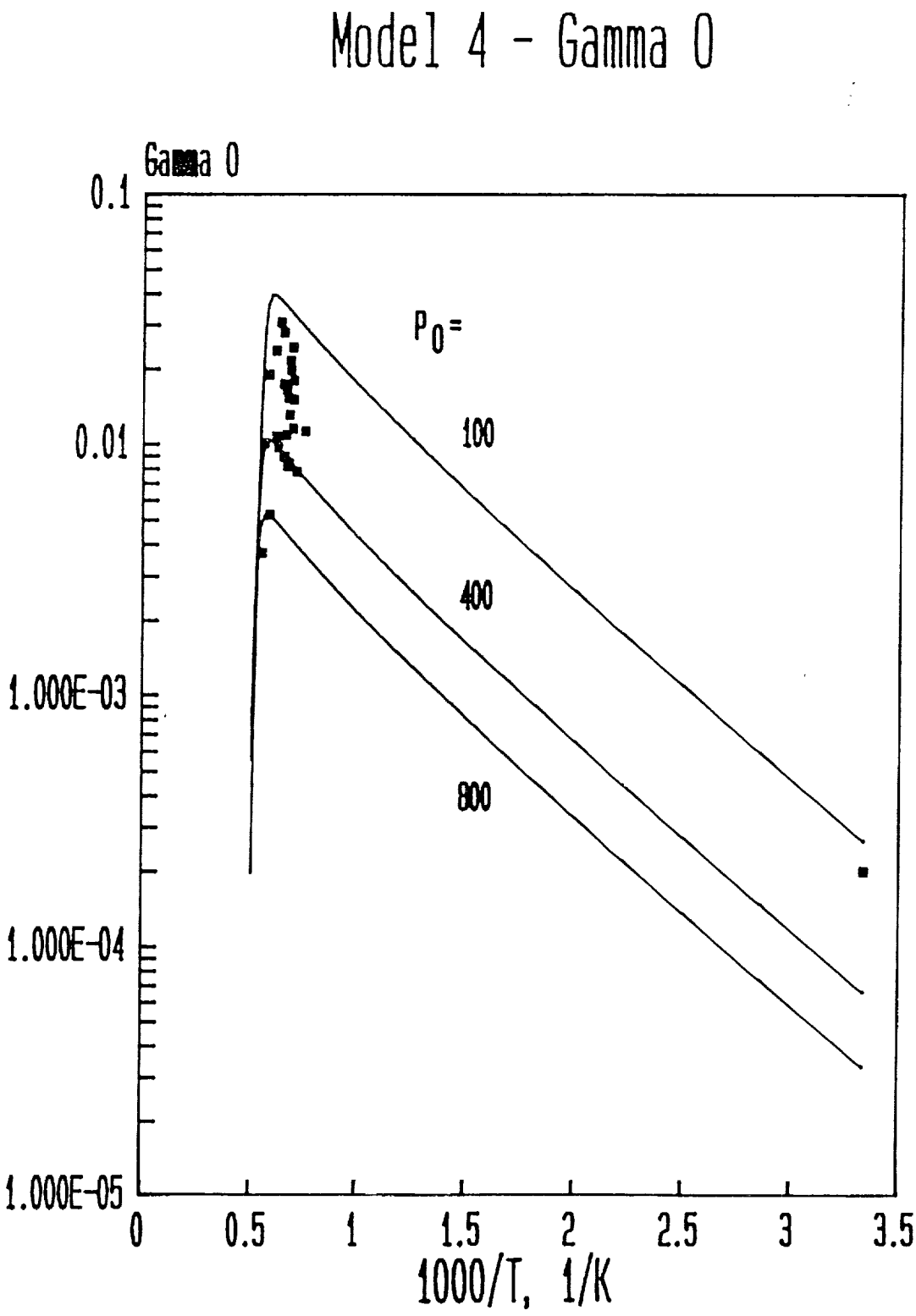

FIGURE 18

Comparison of Model 5 with the Recombination Coefficient
for Oxygen Atoms on RCG Coated HRSI Materials

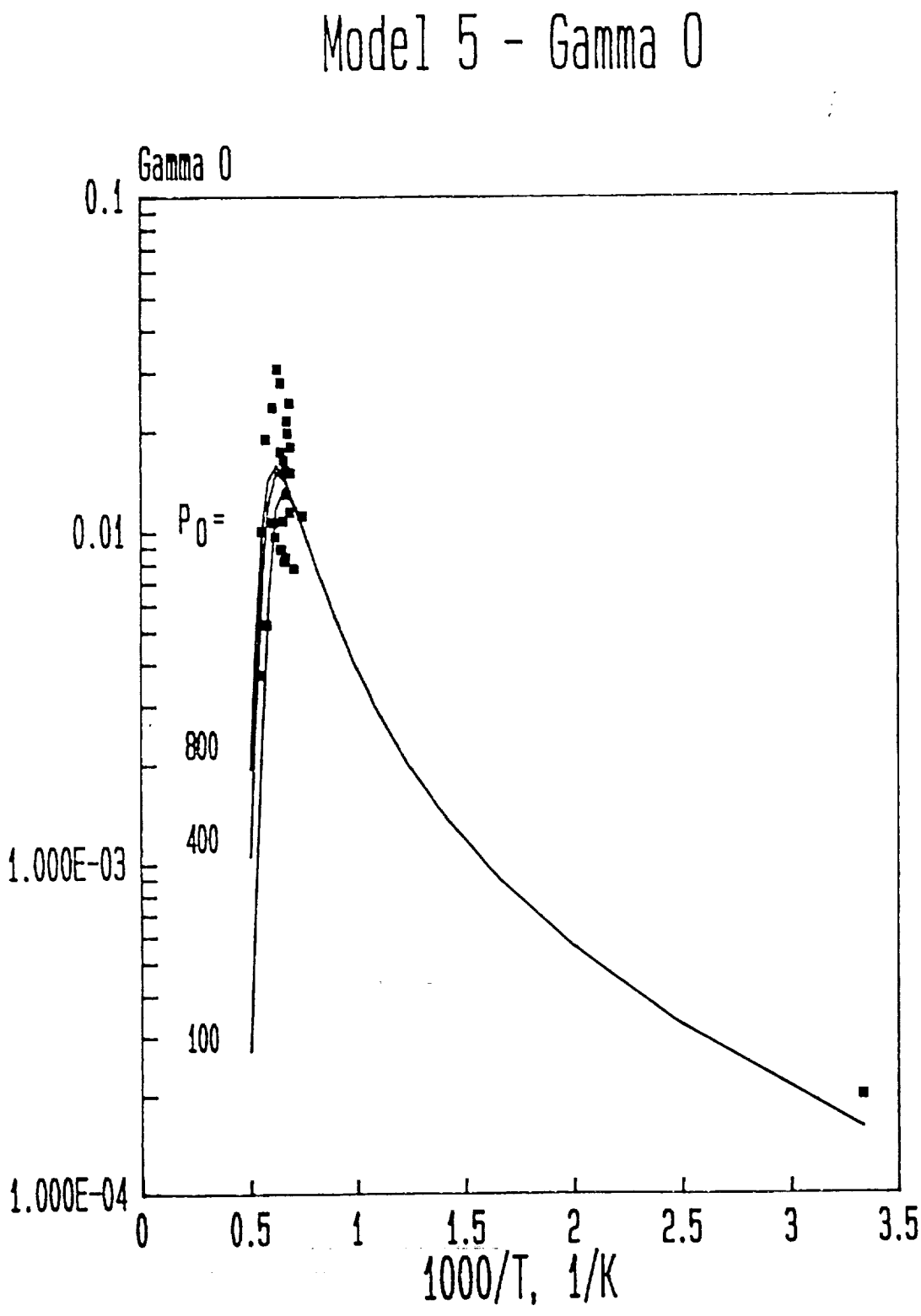

FIGURE 19

Comparison of Model 6 with the Recombination Coefficient
for Oxygen Atoms on RCG Coated HRSI Materials

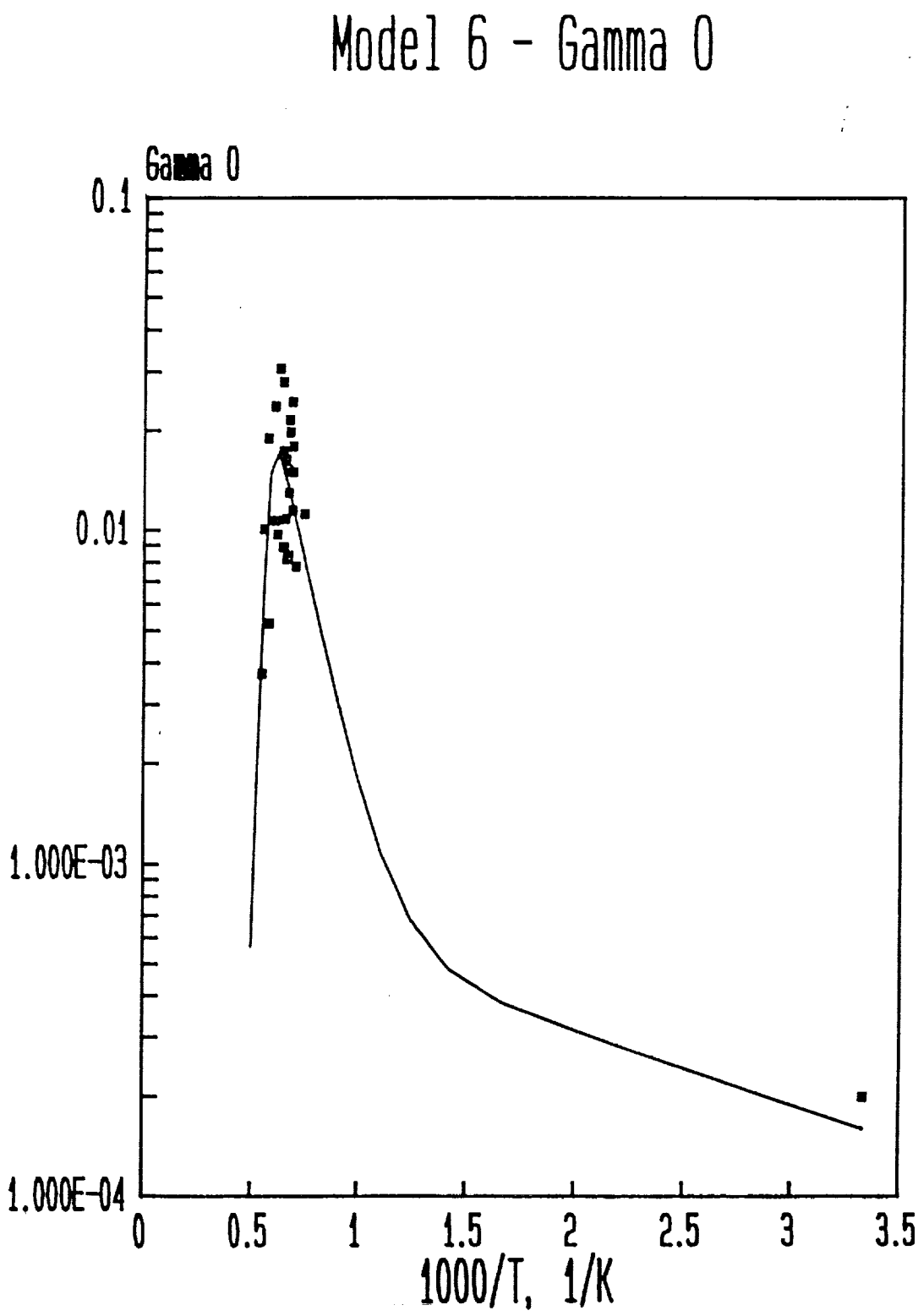

FIGURE 20 A-C

Residual Plots for Various Recombination Models
for Nitrogen Atoms as a Function of 1/T

Residual Plots A-C

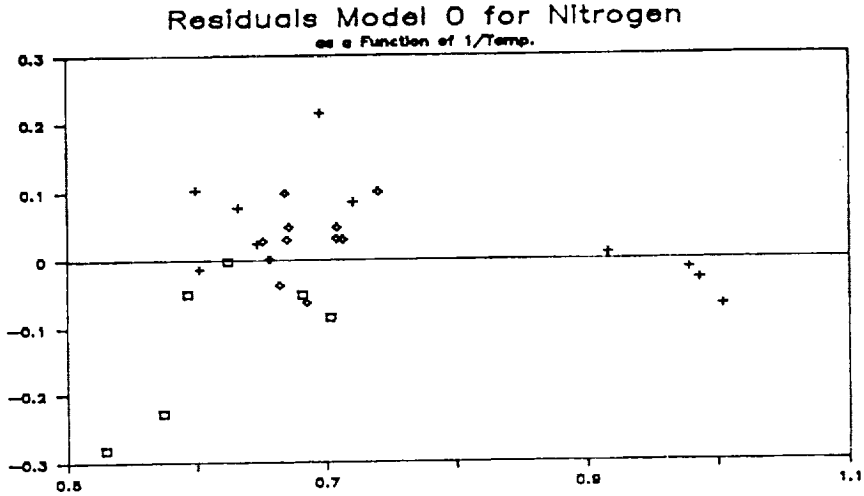

Residual Plot A

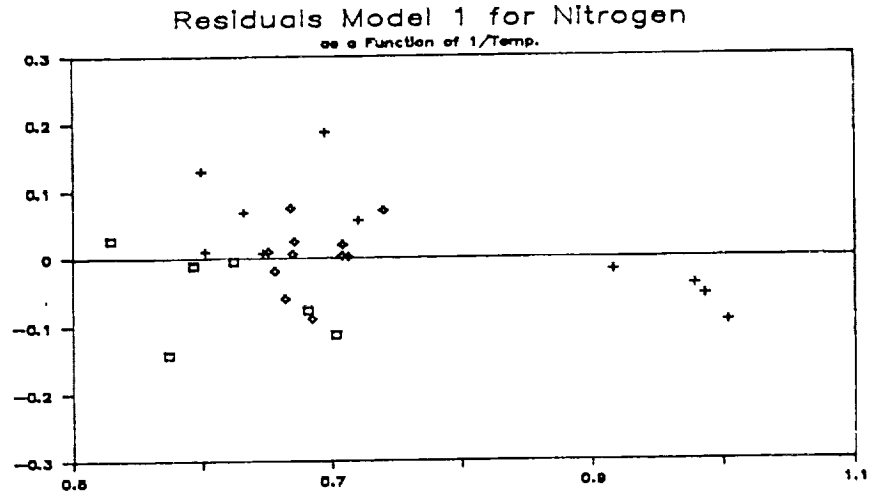

Residual Plot B

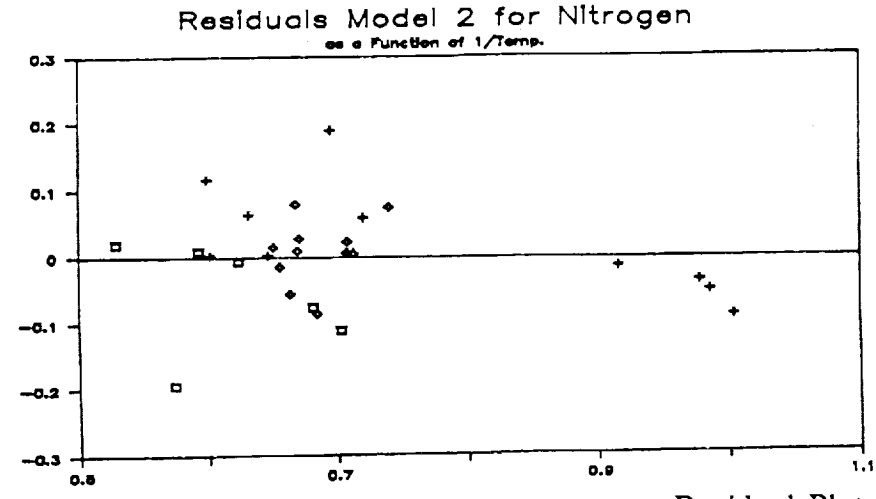

Residual Plot C

FIGURE 20 D-F

Residual Plots for Various Recombination Models
for Nitrogen Atoms as a Function of 1/T

Residual Plots D-F

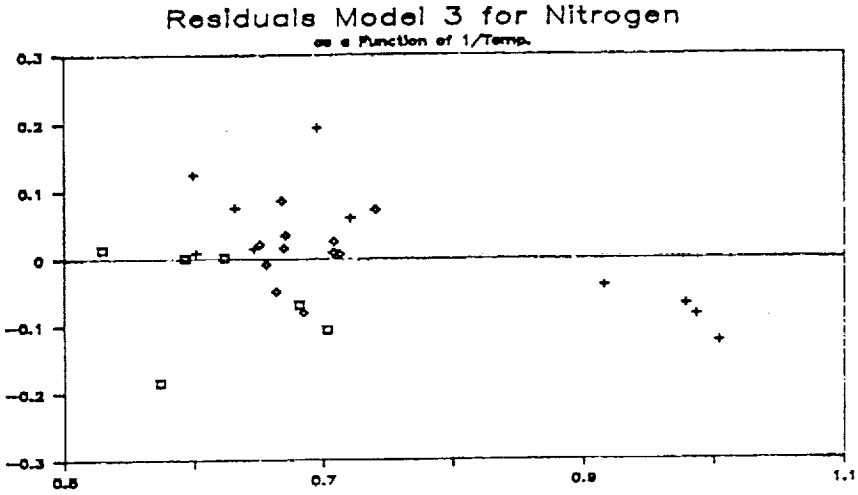

Residual Plot D

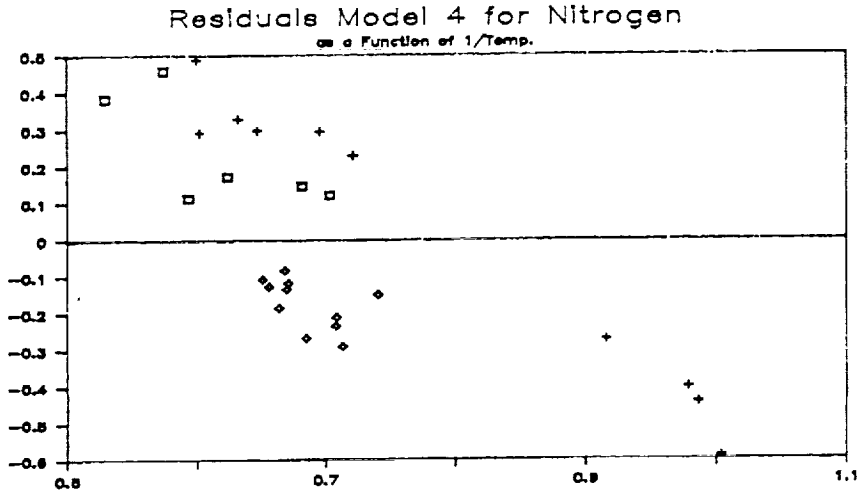

Residual Plot E

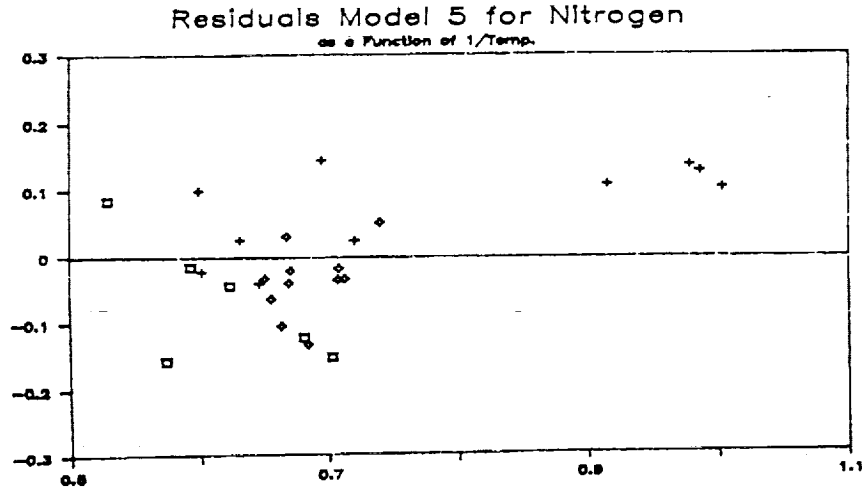

Residual Plot F

FIGURE 20 G

Residual Plots for Various Recombination Models
for Nitrogen Atoms as a Function of 1/T

Residual Plot G

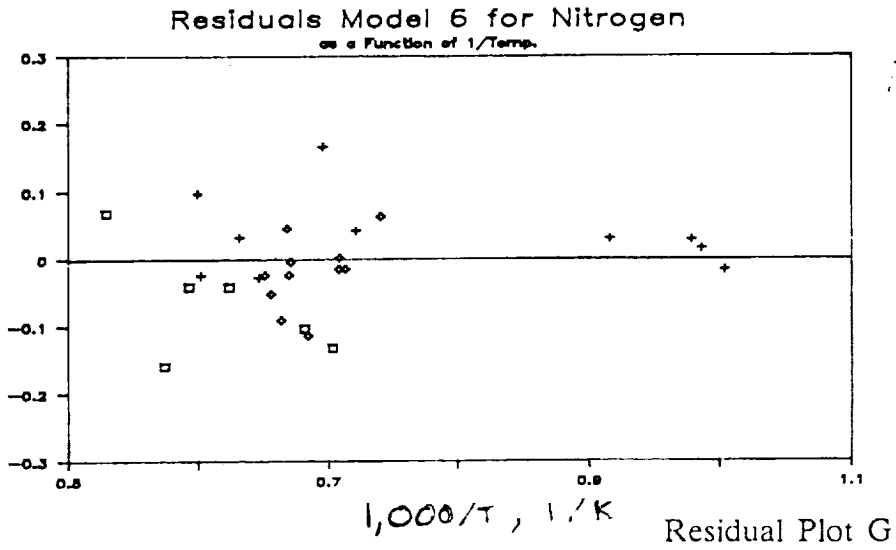

Residual Plot G

Legend for Figure 20 A-G

FIGURE 21 A-C

Residual Plots for Various Recombination Models
for Nitrogen Atoms as a Function of Pressure

Residual Plots A-C

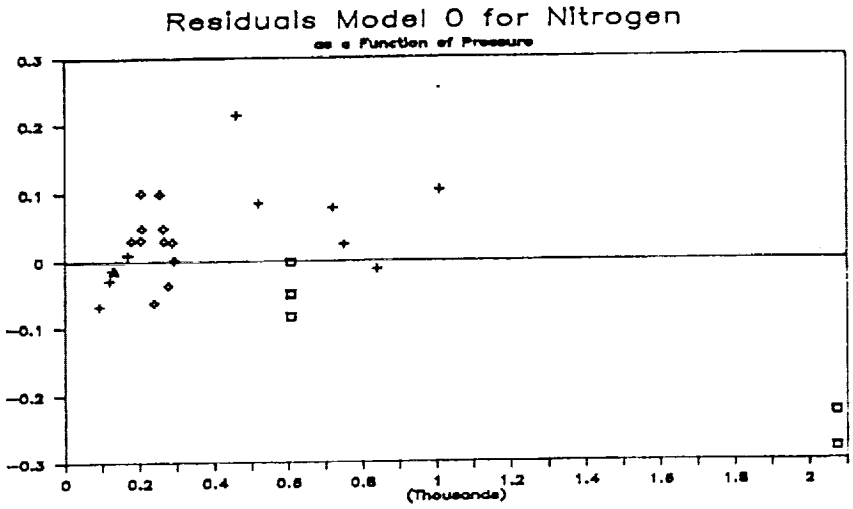

P_N, Pa. Residual Plot A

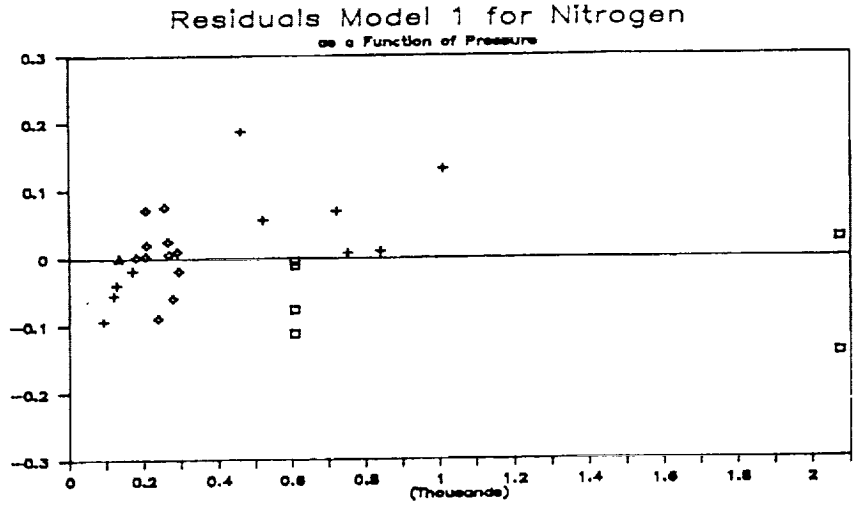

Pressure, P_N, Pa Residual Plot B

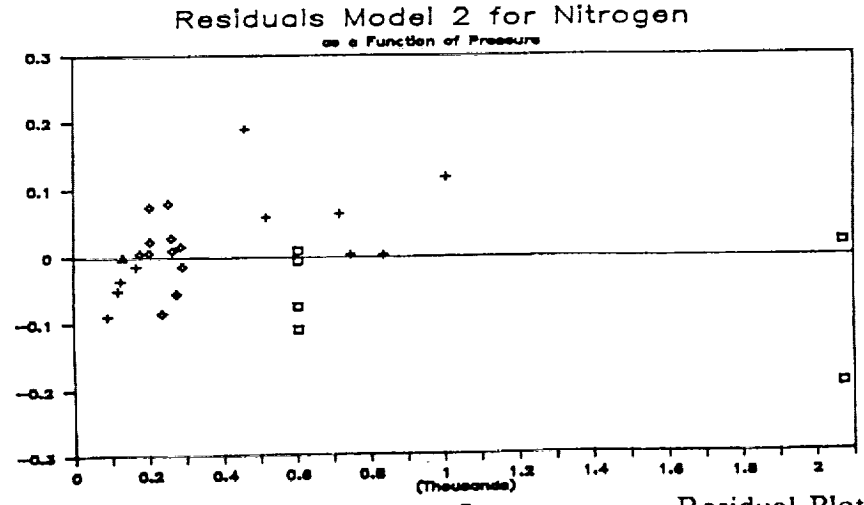

Residual Plot C

FIGURE 21 D-E

Residual Plots for Various Recombination Models
for Nitrogen Atoms as a Function of Pressure

Residual Plots D-E

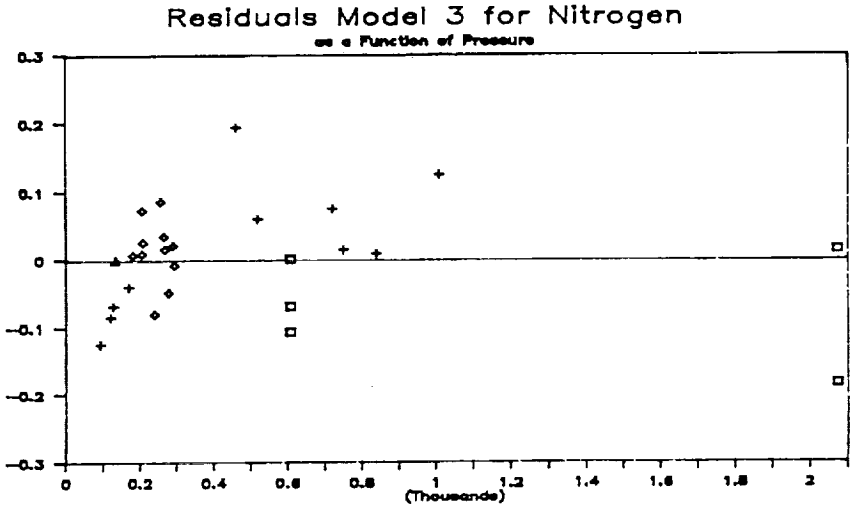

P_N, Pa

Residual Plot D

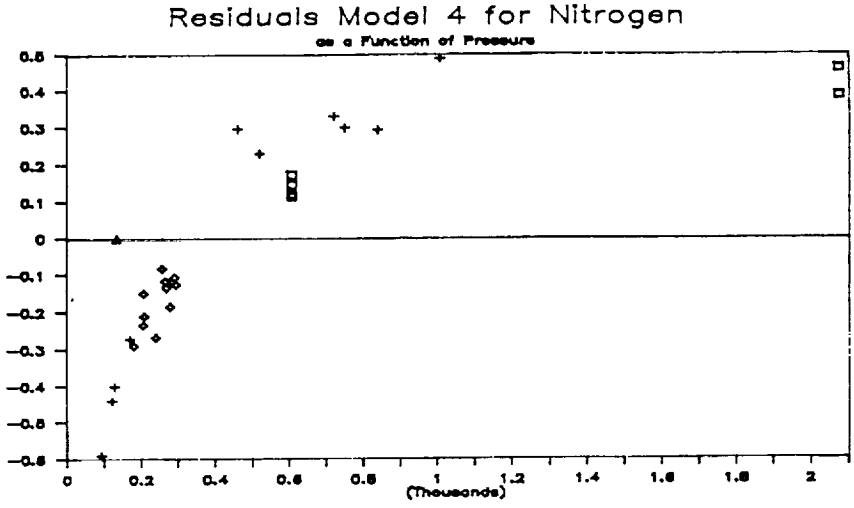

P_N, Pa

Residual Plot E

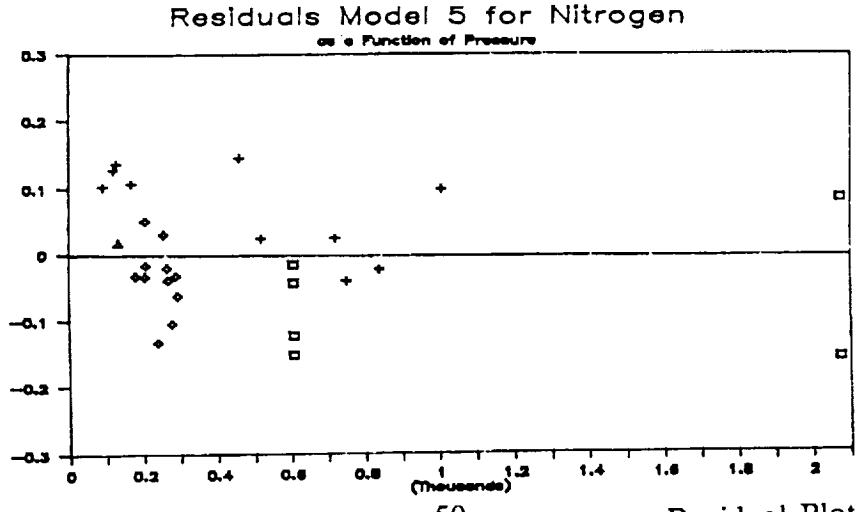

Residual Plot F

FIGURE 21 G

Residual Plots for Various Recombination Models
for Nitrogen Atoms as a Function of Pressure

Residual Plot G

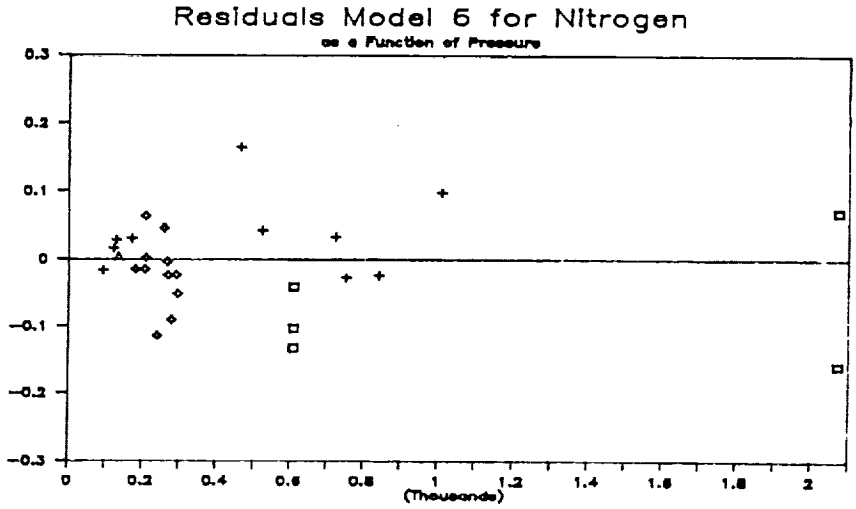

P, Pa

Residual Plot G

Legend for Figure 21 A-G

□ Kaledzdej + Scott ◇ Wiley △ Martinelli

FIGURE 22 A-C

Residual Plots for Various Recombination Models for Oxygen Atoms as a Function of 1/T

Residual Plots A-C

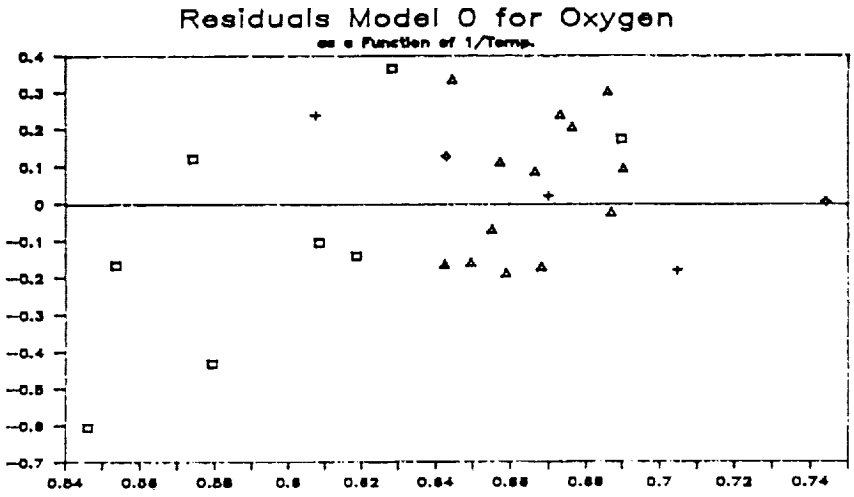

Residual Plot A

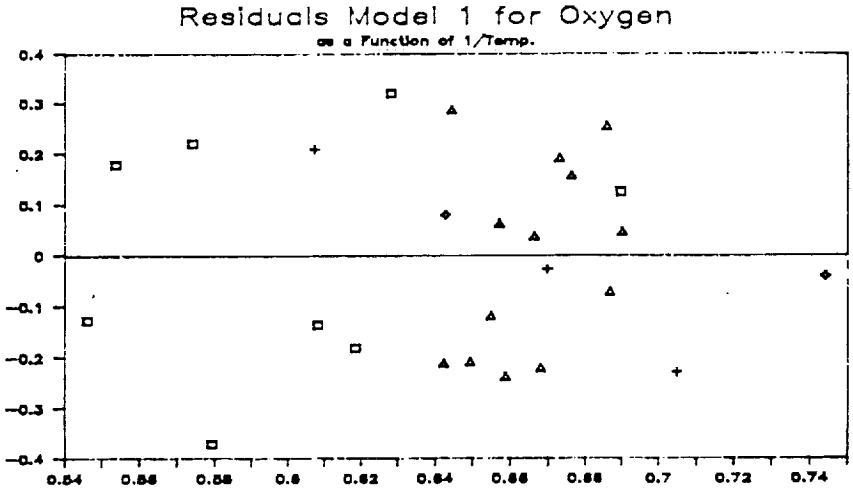

Residual Plot B

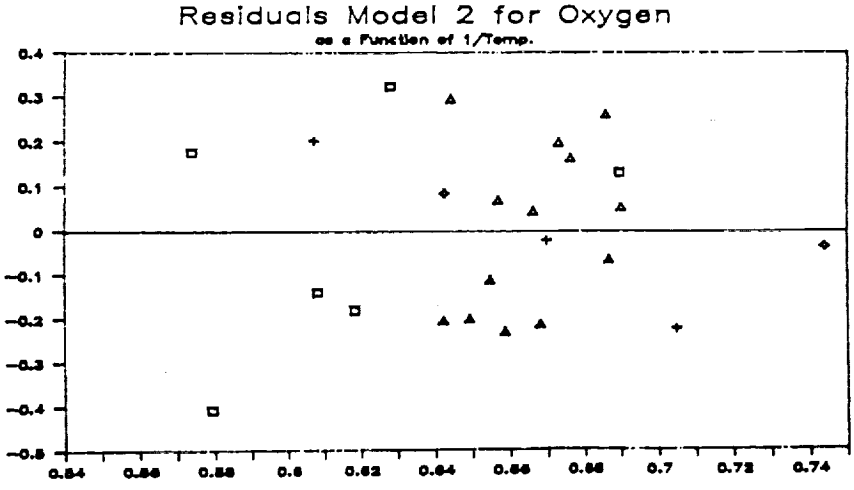

Residual Plot C

FIGURE 22 D-F

Residual Plots for Various Recombination Models
for Oxygen Atoms as a Function of 1/T

Residual Plots D-F

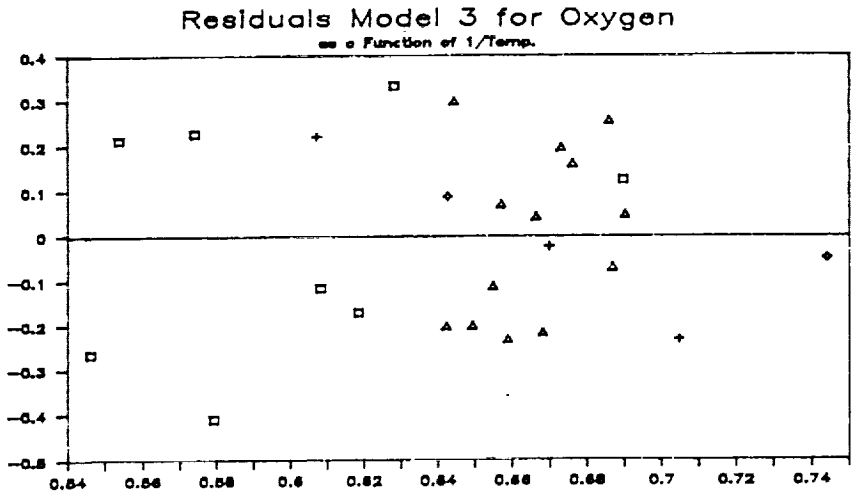

1,000/T, 1/K

Residual Plot D

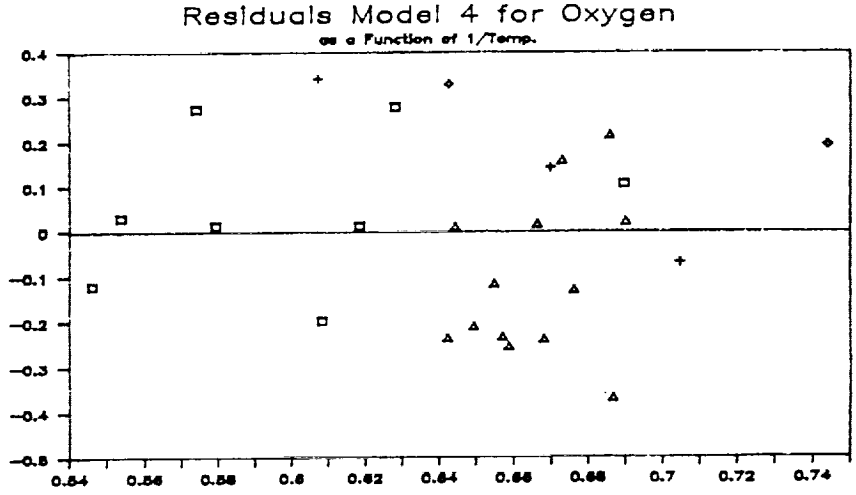

1,000/T, 1/K

Residual Plot E

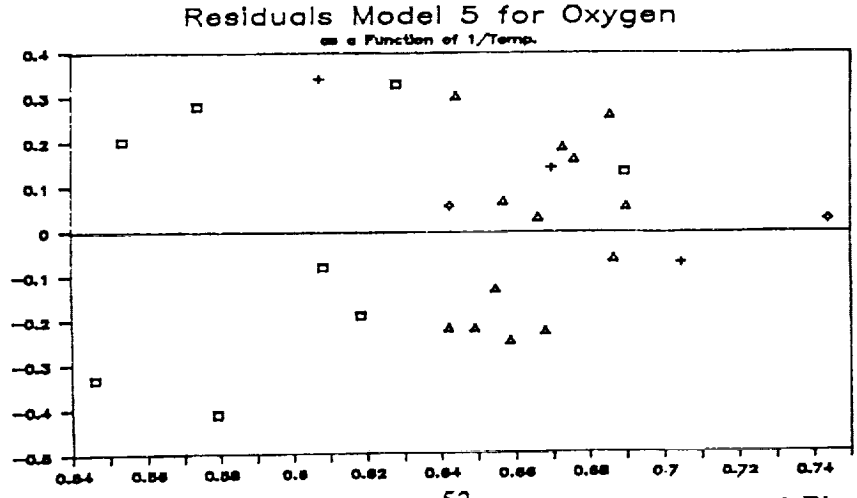

Residual Plot F

FIGURE 22 G

Residual Plots for Various Recombination Models for Oxygen Atoms as a Function of 1/T

Residual Plots G

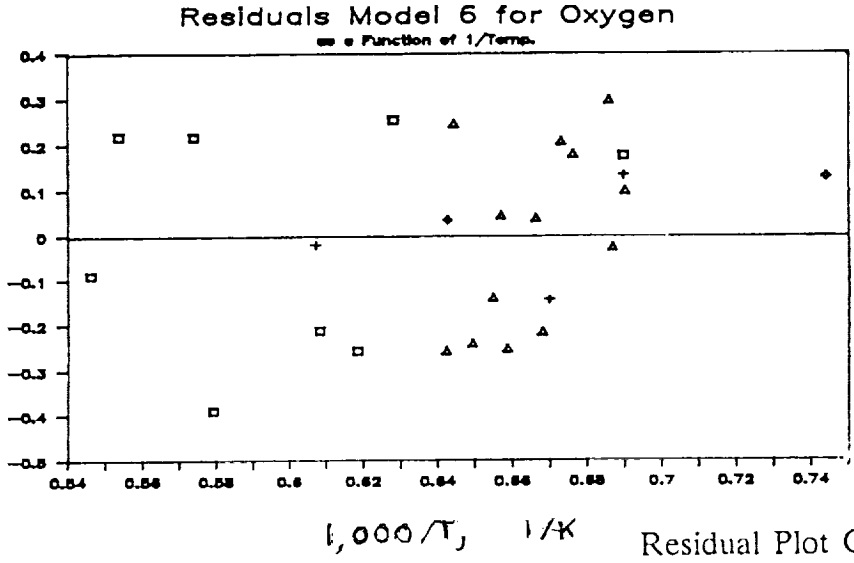

Residual Plot G

Legend for Figure 22 A-G

FIGURE 23 A-C

Residual Plots for Various Recombination Models
for Oxygen Atoms as a Function of Pressure

Residual Plots A-C

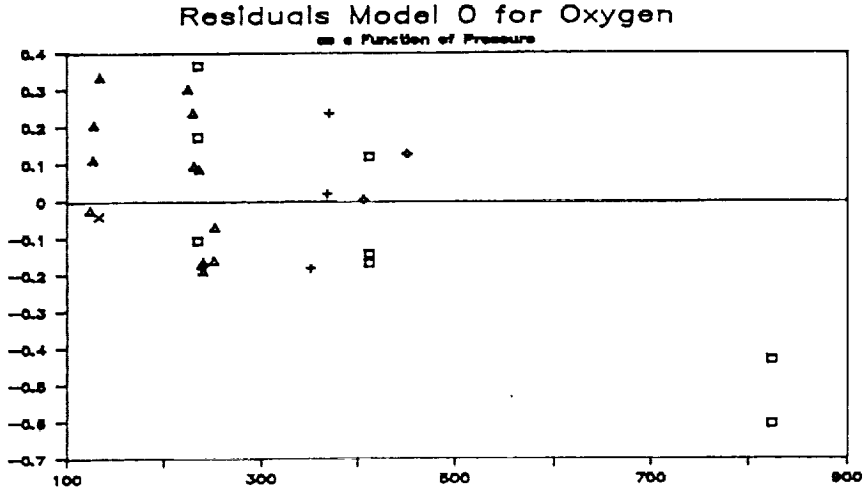

P_o, P_a Residual Plot A

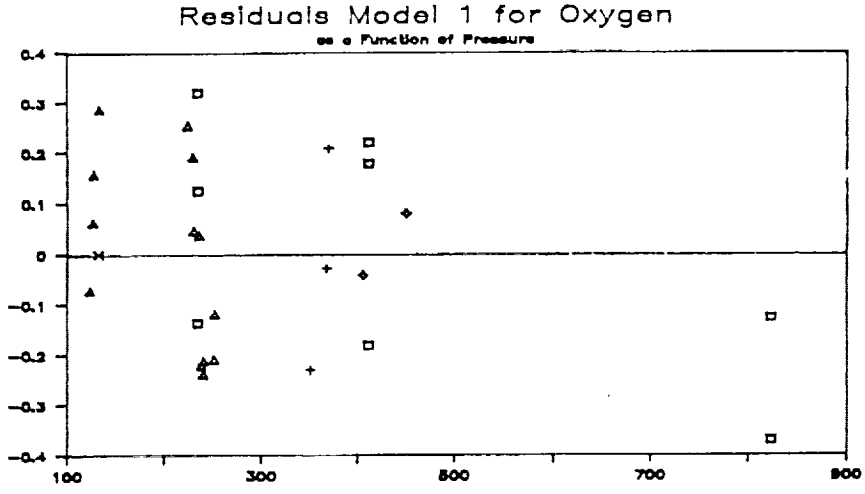

P_o, P_a Residual Plot B

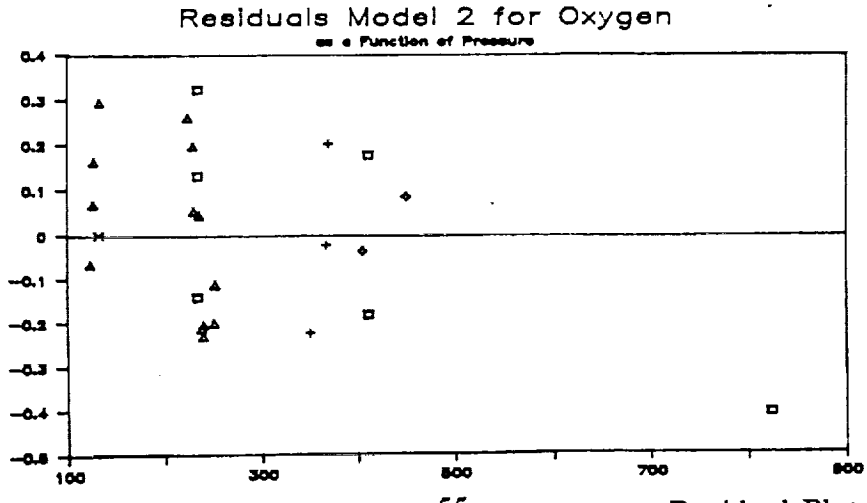

Residual Plot C

FIGURE 23 D-F

Residual Plots for Various Recombination Models
for Oxygen Atoms as a Function of Pressure

Residual Plots D-F

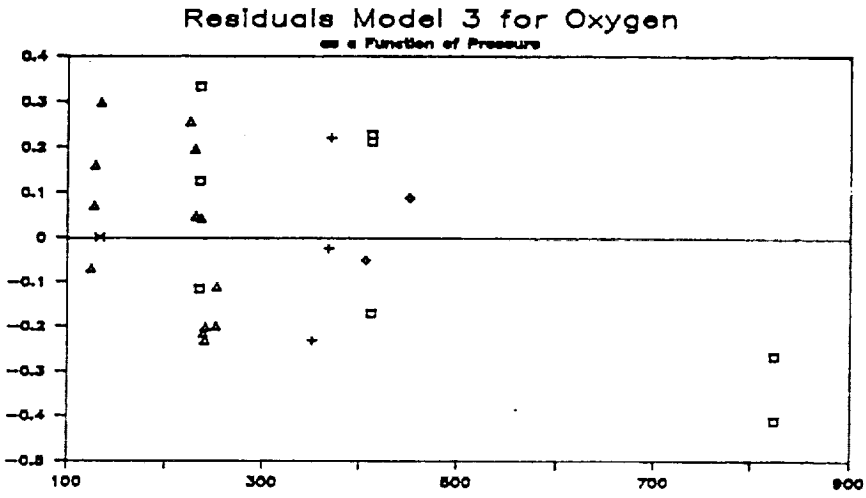

P_o, P_a Residual Plot D

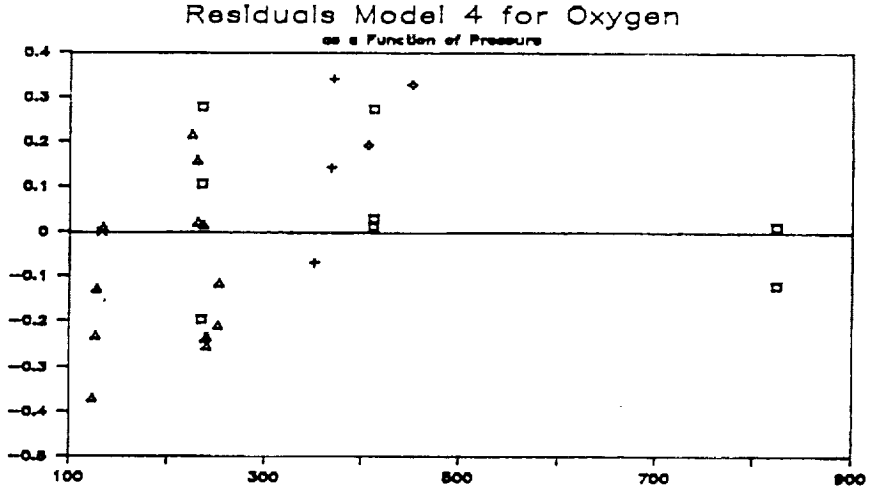

P_o, P_a Residual Plot E

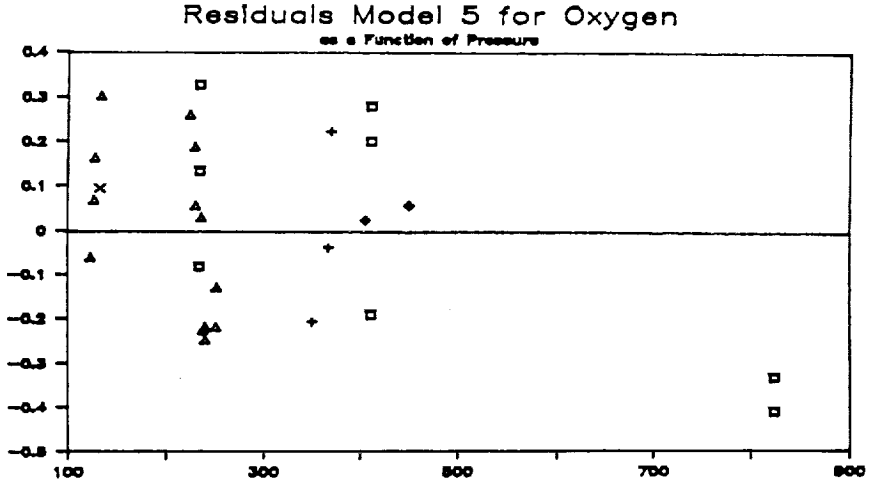

Residual Plot F

FIGURE 23 G

Residual Plots for Various Recombination Models
for Oxygen Atoms as a Function of Pressure

Residual Plot G

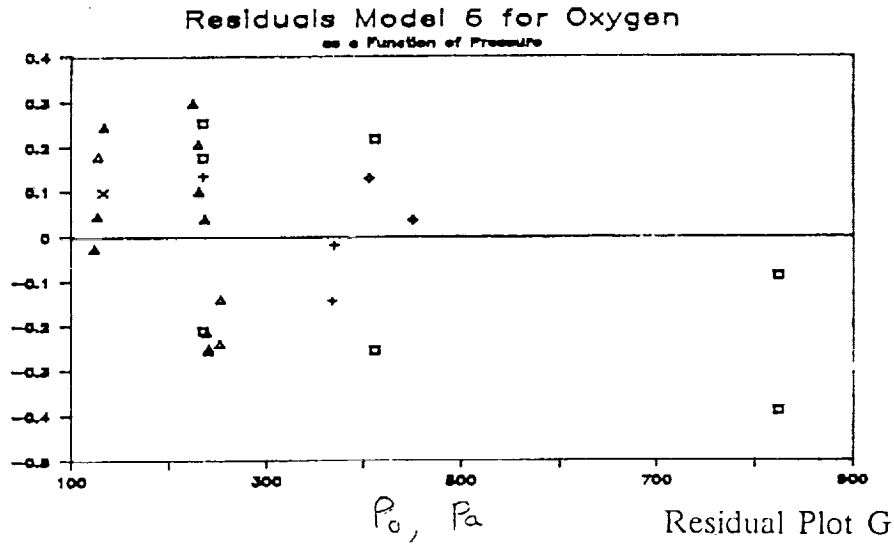

Residual Plot G

Legend for Figure 23 A-G

□ Kolodziej + Scott ◆ Stewart △ Wiley × Marinelli

Applications of Models 1 and 6 to Heating Rate Determination for the Aeroassist Flight Experiment

The application of recombination Models 1 and 6, for the aeroassist flight experiment, to heating rate design as a function of time for reentry trajectory was computed by Mr. Stan Bouslog of Lockheed Engineering and Sciences Company. Comparing the predicted heating rates of Kolodziej and Stewart's (1987) catalytic models, which are discontinuous as a function of temperature, Models 1 and 6, which are continuous models, present slightly higher heating rates earily in the reentry pattern. However, Models 1 and 6 predict much lower heating rates when compared to the fully catalytic wall (shown by the solid curve in both figures). In time, a brief transition occurs where Models 1 and 6 predict a lower heating rate than those predicted by Kolodziej and Stewart due to their lower recombination coefficient. The peak heating rate in both cases occurs about 110 seconds into the reentry trajectory. The maximum heating rate for Models 1 and 6 is about 35 BTU/ft^2/sec, compared to the maximum heating rate of about 33 BTU/ft^2/sec predicted by Kolodziej and Stewart. Thus, the goal of providing design engineers with a continuous recombination model for atom recombination on surfaces has been achieved.

FIGURE 24

Comparison of Stagnation Point Convective Heating Rates for Catalysis Model 1 Compared to Fully Catalytic and Kolodziej and Stewart's Reaction Models

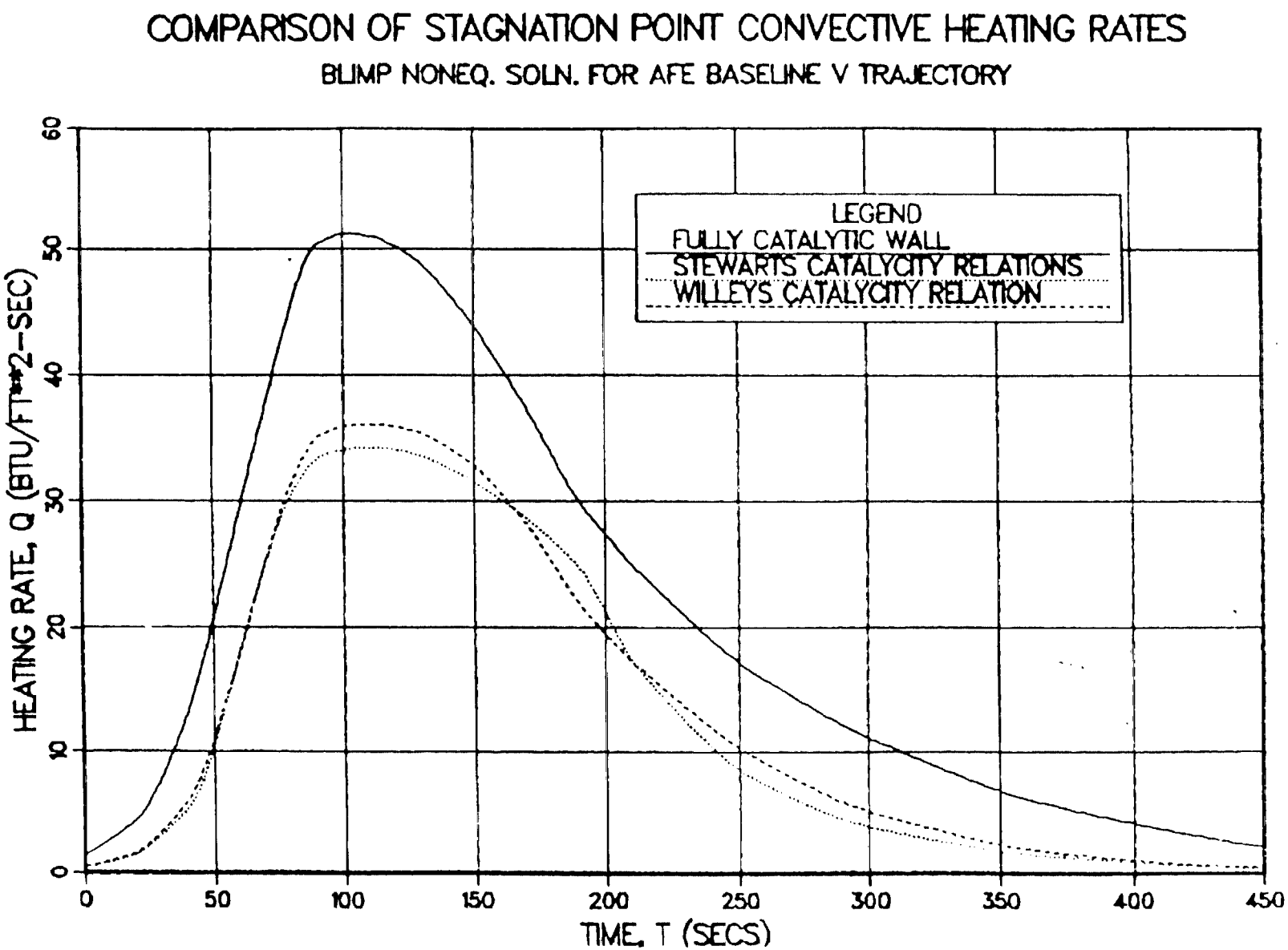

FIGURE 25

Comparison of Stagnation Point Convective Heating Rates for
Catalysis Model 6 Compared to Fully Catalytic and Kolodziej Reaction Models

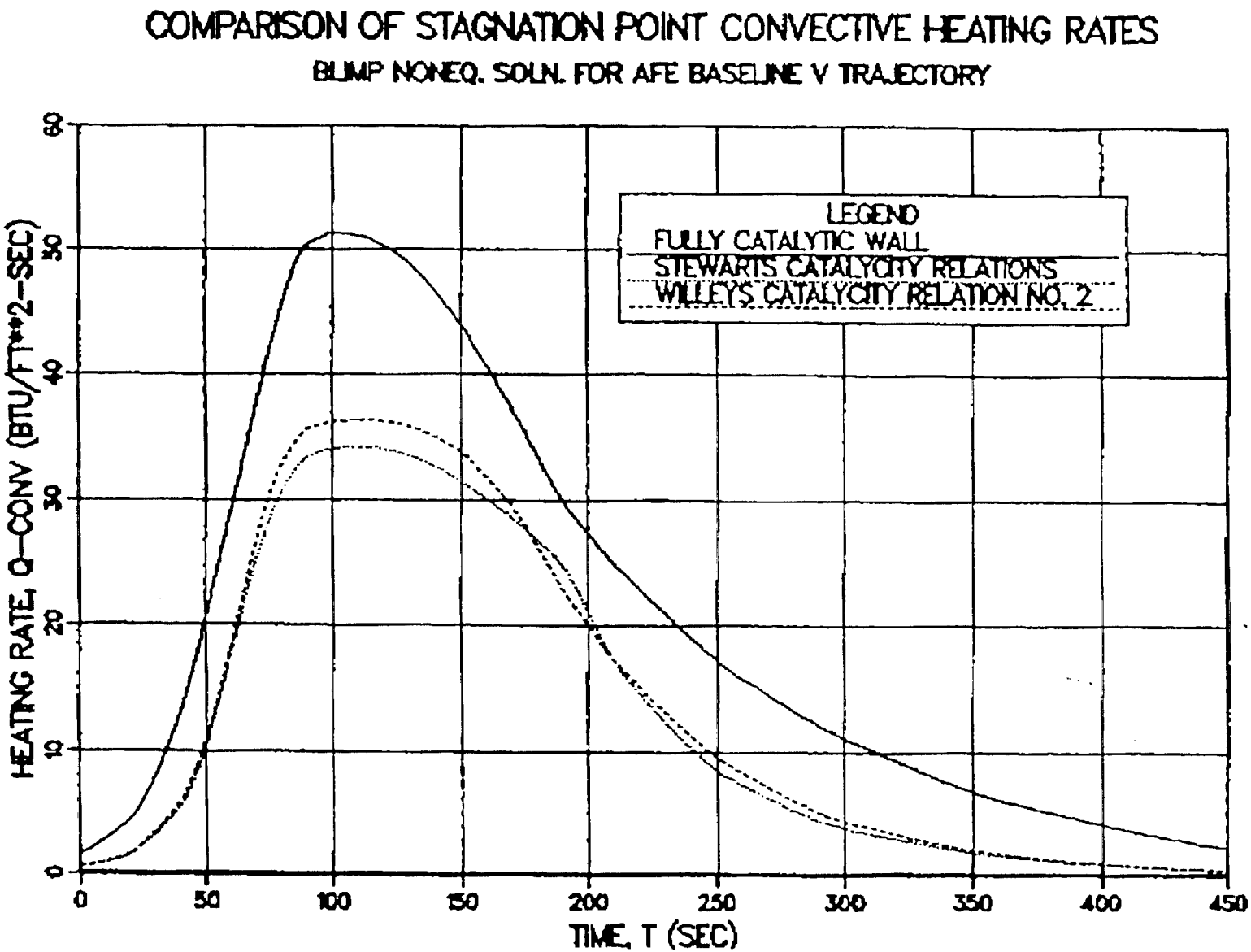

CONCLUSIONS

Recombination models for oxygen and nitrogen atoms on surfaces can be derived from the Rideal-Eley mechanism which describes observed recombination data on RCG coated HRSI surfaces. The most appropriate model was dependent in temperature only and included an adsorption equilibrium term in the numerator and denominator. Normally, Rideal-Eley rate models for recombination coefficients are zero-order in concentration at low temperatures, and first-order at high temperatures; however, available data does not support inclusion of concentration terms into recombination coefficient models. Two recombination models were applied to stagnation point heating rate simulations and illustrate similar heating rates to those achieved by catalytic relations discontinuous in temperature. Parameter estimation in all of the models is difficult, requiring reparameterization and possible pre-determination of some constants. More experiments are recommended to verify these conclusions.

RECOMMENDATIONS

More experimental work is recommended in two temperature ranges, 300 to 1000 K and 1500 to 1800 K, regarding atomic recombination rates on RCG coated HRSI materials. Additional experiments which vary the partial pressure of atoms at the surface are also necessary. In summary, depending upon the results, one of the four models presented above can be used. If additional experiments support no concentration dependency, then Model 1 or Model 6 should be chosen (Model 6 if the apparent activation energy increases in the temperature range from 300 to 1400 K, Model 1 if the constant activation energy occurs from 300 to 1400 K). If concentration dependence is found, then Model 2 or Model 4 should be chosen (Model 2 if the recombination coefficient is found to be zero-order at low temperatures and first-order at high temperatures, Model 4 if the recombination coefficient is found to be negative first-order and transitions to first-order as temperature increases).

ACKNOWLEDGEMENTS

The author would like to thank Caryn Vigoda for her help in editing this report. The author acknowledges Mr. David J. Blake, M.S., Chemical Engineering, Department of Chemical Engineering, 1989, for his assistance in the creation of the data base and early data evaluation of Rideal-Eley and Langmuir-Hinshelwood reaction. The author also appreciates the assistance of Mr. Stan Bouslog and the Lockheed Engineering and Sciences Company for the evaluation of reaction models in terms of the AFE baseline trajectory heating rates. Mr. Stanley H. Goldstein and Dr. Richard Bannerot are acknowledged for their assistance in providing the funding for this work under the NASA grant #NAG-9-314. And, finally, Dr. Carl Scott is most gratefully acknowledged for his advice and assistance throughout the project.

REFERENCES

Back, R. A. and Others, "The Decay of Active Nitrogen at High Temperature," Canadian Journal of Chemistry, Vol. 37, 1959, pp. 2059-2063 (from Newman).

BMDP Statistical Software, W. J. Dixon, Ed., University of California Press, Berkeley, CA, 1983.

Breen, J. and Others, "Catalysis Study for Space Shuttle Vehicle Thermal Protection Systems," NASA CR-134124, 1973.

Draper, N. and Smith, H., Applied Regression Analysis, 2nd Ed., John Wiley & Sons, NY, 1981.

Evenson, K. M. and Burch, D. S., "Atomic-Nitrogen Recombination," J. Chem. Phys., Vol. 45, 1966, pp. 2450-2460 (from Newman).

Ghosh, S. N. and Jain, S. K. "Catalytic Efficiency of Pyrex Glass for the Recombination of Nitrogen Atoms," Brit. J. of App. Phys., Vol. 17, 1966, pp. 765-767.

Goulard, R., "On Catalytic Recombination Rates in Hypersonic Stagnation Heat Transfer," Jet Propulsion, Vol. 28, Nov. 1958, pp. 737-745.

Kelly, R. and Winklea, C. A., "The Kinetics of the Decay of Nitrogen Atoms as Determined from Chemical Measurements of Atom Concentrations as a Function of Pressure," Can. J. of Chem., Vol. 37, 1959, pp. 62-78 (from Newman).

Kolodziej, P. and Stewart, D. A., "Nitrogen Recombination on High-Temperature Reusable Surface Insulation and the Analysis of its Effects on Surface Catalysis," AIAA-87-1637, June 1987.

LOTUS 123 Reference Manual Release 2, Lotus Development Corp., Cambridge, MA 1985.

Marinelli, W. J., and Campbell, J. P., "Spacecraft-Metastable Energy Transfer Studies: Final Report," NAS9-17565, July 1986 (from Newman).

Marinelli, W. J., "Collisional Quenching of Atoms and Molecules on Spacecraft Thermal Protection Surfaces," AIAA 88-2667, June 1988.

Marshall, T. C. and Others, "Molecular Storage and Transfer of Electromagnetic Energy in Gaseous Plasmas: Final Report," RADC-TDR-63-275, 1964 (from Newman).

Newman, M., "A Model for Nitrogen Atom Recombination on a Silicon Dioxide Surface," M.S. Thesis, Air Force Institute of Technology, AFIT(GE)ENG/87D-50, 1987.

Outred, M. and Pillow, M. E., "The Logarithmic Decay of the Leur's-Raleigh Afterglow in Nitrogen," J. of Phys. B-- Atomic and Molecular Physics, Vol. 3, 1970, pp. 399-404 (from Newman).

Rahman, J. L. and Linnett, J. W., "Recombination of Atoms at Surfaces. Part 10 -- Nitrogen Atoms at Pyrex Surfaces," Trans. of the Faraday Soc., Vol. 67, 1971, pp. 170-178.

Rakich, J. V., Stewart, D. A., & Lanfranco, M. J., "Results of a Flight Environment on the Catalytic Efficiency of the Space Shuttle Heat Shield," AIAA 82-0944, June 1982.

Rochelle, W. C., Ting, P. C., Mueller, S. R., Colovin, J. E., & Bouslog, S. A., "Aerobrake Heating Rate Sensitivity Study for the Aeroassist Flight Experiment (AFE)," AIAA-89-1733, June 1989.

Rosner, D. E. and Feng, H., J. of the Chem. Soc. Faraday Trans. I, Vol. 79, 1974, pp. 889-907.

Sancier, K. M. and others, "Luminescence of Solids Excited by Surface Recombination of Atoms. II. Recombination Coefficients," J. of Chem. Phys., Vol. 37, 1962, pp. 860-864 (from Newman).

Scott, C. D., "Catalytic Recombination of Nitrogen and Oxygen on High-Temperature Reusable Surface Insulation," Aerothermodynamics and Planetary Entry, ed. by A. L. Crosbie, Vol. 77, Prog. in Astro. and Aero.: 1981, pp. 192-212.

Scott, C. D., "Effects of Nonequilibrium and Wall Catalysis on Shuttle Heat Transfer," J. of Spacecraft and Rockets, Vol. 22, No. 5, 1985, pp. 489-499.

Scott, C. D. and Derry, S. M. "Catalytic Recombination and the Space Shuttle Heating," AIAA-82-0841, 1982.

Seward, W. A., "A Model for Oxygen Atom Recombination on a Silicon Dioxide Surface," Ph.D. Thesis, Air Force Institute of Technology, AFIT/DS/AA/85-1, 1985.

Shuman, M. E. and Brennen, W., "Heterogeneous Recombination of Nitrogen Atoms by the Smith Side Tube Method: Effects of Tube Length and Homogeneous Recombination," J. Chem. Phys., Vol. 68, 1978, pp. 4077-4085 (from Newman).

Stewart, D. A., Henline, W.D., Kolodziej, P. I., and Pincha, E. M. W., "Effects of Surface Catalysis on Heating to Cermaic Coated Thermal Protection Systems for Transatmospheric Vehicles," AIAA-88-2706, June 1988.

Stewart, D.A., Rakich, J. V., Lanfranco, M. J., "Catalytic Surface Effects Experiment on the Space Shuttle," Thermophysics of Atomos. Entry, ed. by T. E. Horton, Vol. 82, Prog. in Astro. and Aero.: 1982, pp. 248-272.

Ting, P. C., Rochelle, W. C., Mueller, S. R., Colovin, J. E., Scott, D. D., and Curry, D. M., "Development of AFE Aerobrake Aerothermodynamic Data Book," AIAA-89-1734, June 1989.

Wentink, T. Jr. and Others, "Nitrogen Atomic Recombination at Room Temperature," J. Chem. Phys., Vol, 29, 1958, pp. 231-232 (from Newman).

Willey, R. J., "Arc Jet Diagnostics Tests, Final Report," NASA-JSC/ASEE SFFP, 1988.

Yamashita, T. "Rate of Recombination of Nitrogen Atoms," J. Chem. Phys., Vol. 70, 1979, pp. 4248-4258 (from Newman).

Young, R. A., "Pressure Dependence of the Absolute Catalytic Efficiency of Surfaces for Removal of Atomic Nitrogen," J. Chem. Phys., Vol. 34, 1961, pp. 1292-1294 (from Newman).

LIST OF NOMENCLATURE

A_N	Area normal to flux of atoms, m^2
c	Average velocity of a gas molecule or atom, m/sec
C_a	Concentration of surface sites in Seward Model, sites/m^2
D	Equilibrium activation energy for adsorption, J/atom or kJ/g mole
Ea	Activation energy for Rxn.-A-2, J/atom or kJ/mole
h	Planck's constant, 6.6256 E-34 N-M sec
K	Equilibrium constant for Reactions A1 & B-1, m^3/atom
k_0	Arrhenius preexponential constant for Equation 1a, unitless
k_{-10}	Arrhenius preexponential constant for k_{-10} Rxn. A-1 & B-1, 1/sec
k_1	Forward reaction rate constant in Rxns. A-1 & B-1, m^3/sec site
k_2	Forward reaction rate constant in Rxns. A-2 & B-2 m^3/sec site
k_3	Forward rate constant used in Model 6, unitless
k_{2o}	Arrhenius preexponential constant for k_2 in Rxns. A-2 & B-2 m^3/sec site
k_{30}	Arrhenius preexponential constant for k_3, unitless
Ka	Arrhenius preexponential constant for K in Rxns. A1 & B1 m^3/atom
k_B	Boltzmann Constant, 1.38 E-23 N-m/K atom
k_w	First-order rate constant, m/sec
m	Mass of an atom, kg/atom
N	Nitrogen atoms
[N]	Concentration of nitrogen atoms, atoms/m^3
N_O	Surface impingement rate of atoms as given by kinetic theory, atoms/m^2sec
O	Oxygen atoms
[O]	Concentration of oxygen atoms, atoms/m^3
[OS]	Concentration of adsorbed oxygen atoms, atoms/m^2
P	Steric factor in Eqn. A-19 = P_o exp (P_2T)
P_0	Preexponential factor for P
P_2	Exponential factor for P
P_i	Partial pressure of gas species i, Pa
P_t	Total pressure, Pa
R	Universal Gas Constant 8,314 kJ/kg mole/K or 0.0008314 kJ/g mole K
[S]	Concentration of reduced sites on the surface, atoms/m^2
S_0	Concentration of total sites on the surface, atoms/m^2
S_{01}	Preexponential constant in So
S_1	Exponential factor in So
So	Sticking coefficient in Eqn. A-19 = S_{01} exp (S_1T)
t	time, s
T	Temperature at surface, K
T_W	Temperature at the tile surface, K
ς	delta, thermal desorption coefficient in Eqn. A-19
γ_i	gamma, recombination coefficient
σ	Stefan-Boltzmann constant

APPENDIX A

Derivation of Rideal-Eley Mechanistic Models

The basic rate equations are:

Adsorption of oxygen onto the surface:

$$O + [S] \underset{k_{-1}}{\overset{k_1}{\rightleftharpoons}} [OS] \qquad \text{A-1}$$

Reaction of a surface oxygen with a gas phase oxygen:

$$Og + [OS] \xrightarrow{k_2} O_2 + [S] \qquad \text{A-2}$$

Where [S] is the concentration of "reduced" surface sites, sites/m^2
and where [OS] is the concentration of "oxidized" surface sites, atoms/m^2.

Based on the law of mass action, the rate of O_2 production per unit area is proportional to the concentration of oxygen in the gas phase times the concentration of oxide sites:

$$d\ O_2/A_N dt = k_2\ [O]\ [OS] \qquad \text{A-3}$$

where [O] is in atoms/m^3 and k_2 has the units m^3/sec atom.

At steady state the rate of surface oxide, [OS], site formation has to equal zero:

$$d[OS]/A_N dt = 0 = k_1\ [O][S]-k_{-1}[OS]-k_2[O][OS] \qquad \text{A-4}$$

If the number of total surface sites are constant then

$$[S_0]=[S] + [OS] \qquad \text{A-5}$$

or

$$[S] = [S_0]-[OS] \qquad \text{A-6}$$

Substitution of Equation A-6 into Equation A-4 leads to the following equation:

$$d[OS]/A_N\ dt=0=k_1[O][S_0]-k_1[O][OS]-k_{-1}[OS]-k_2[O][OS] \qquad \text{A-7}$$

[OS] can be factored and a solution found for [OS] in terms of rate constants, gas phase concentration, and catalyst site concentration results.

$$[OS] = k_1[O][S_0]/(k_1[O]+k_{-1}+k_2[O]) \quad \text{A-8}$$

Substitution of Equation A-8 into Equation A-3 leads to:

$$dO_2/A_N\ dt=k_1k_2[O]^2[S_0]/(k_1[O]+k_{-1}+k_2[O]) \quad \text{A-9}$$

Gamma O, γ_o , is defined as the number of atoms reacting on the surface divided by the number of atoms which strike the surface:

$$\gamma_o=-dO/A_N\ dt/N_O \quad \text{A-10}$$

By reaction stoichiometry:

$$O+O \rightleftharpoons O_2 \quad \text{A-11}$$

or in terms or rates,

$$-1/2\ dO/dt = dO_2/dt \quad \text{A-12}$$

or

$$dO/dt = -2\ dO_2/dt \quad \text{A-13}$$

Substitution of Equation A-13 into Equation A-10 results in:

$$\gamma_o = 2\ dO_2/A_N\ dt/N_O \quad \text{A-14}$$

or

$$\gamma_o = 2\ k_1k_2[O]^2[S_0]/(k_1[O]+k_{-1}+k_2[O])/N_O \quad \text{A-15}$$

From the kinetic theory of gases

$$N_O=[O]c/4=[O][k_BT/2m\pi]^{1/2} \quad \text{A-16}$$

where

$$c \text{ is the average velocity per particle } = [8k_BT/m\pi]^{1/2} \quad \text{A-17}$$

and

[O] is the number density of atoms, atoms/m^3

Substitution of Equation A-16 into Equation A-15 results in the following:

$$\gamma_o=2k_1k_2[O][S_0][2m\pi/k_BT]^{1/2}/(k_1[O]+k_{-1}+k_2[O]) \quad \text{A-18}$$

Discussion: Equation A-18 is analogous to recombination models derived by Seward (1985) for oxygen recombination and Newman (1987) for nitrogen recombination.

Seward's model is as follows:

$$\gamma_o = 2PN_O So \exp(-Ea/k_B T)/(N_O So + \zeta + PN_o \exp(-Ea/k_B T) \qquad \text{A-19}$$

By factoring [O] in Equation A-18 and N_O in Equation A-19 the equations can be compared.

$$\gamma_o = 2k_1 k_2 [So](2m/k_B T)^{1/2}/(k_1 + k_{-1}/[O] + k_2) \qquad \text{A-20}$$

and

$$\gamma_o = 2\ P\ So \exp(-Ea/k_B T)/(So + \zeta/N_O + \exp(-Ea/k_B T)) \qquad \text{A-21}$$

Thus the adsorption term in Equation A-1 is equivalent to So

$$k_1 = So \qquad \text{A-22}$$

likewise

$$k_{-1}/[O] = \zeta/N_o \qquad \text{A-23}$$

and

$$k_2 = P \exp(-E/k_B T) \qquad \text{A-24}$$

In conventional kinetics, each rate constant, k_i, can be described by an Arrhenius expression:

$$k_i = k_{io} \exp(-E_i/k_B T) \qquad \text{A-25}$$

A comparison of Equation A-20 and A-21 can be made by placing the Arrhenius definitions on the left hand side of equations A-22, A-23 and A-24 and the definitions given in Seward (1985) and Newman (1987) for the terms on the right hand side. Thus,

$$k_{10} \exp(-E_1/k_B T) = S_{01} \exp(-0.002\ T) \qquad \text{A-26}$$

The left hand side predicts that will increase with temperature while the right hand side predicts that will decrease slightly with temperature. <u>This is the major difference between the two models.</u>

$$k_{-10} \exp(-D/k_BT)/[O] = C_a(k_BT/h)\exp(-D/k_BT)/N_O \quad \text{A-27}$$

or

$$k_{-10}/[O] = C_a(k_BT/h)/[O](k_BT/2m\pi)^{1/2} \quad \text{A-28}$$

or

$$k_{-10} = C_a\,(k_BT2m\pi)^{1/2}/h \quad \text{A-29}$$

Equal within a constant with a small influence of temperature

and

$$k_{20} \exp(-Ea/k_BT) = P \exp(-Ea/k_BT) \quad \text{A-30}$$

or

$$k_{20} = P$$

In Seward's work P is a function of temperature $P_0 \exp(P_2T)$ until P exceeds 0.1 where it is set equal to 0.1. Therefore, k_{20} is within a constant factor of P at higher temperatures.

Simplification of Equation A-18

Often the temperature term $[2m\pi/k_BT]^{1/2}$ is assumed approximately constant in the temperature range of interest as compared to the exponential terms, and is combined with a preexponential constant in the Arrhenius equation. If the rate of reaction A-2 is rate limiting, $k_2[O]$ is much lower compared to k_{-1} and $k_1[O]$ in the denominator and the term is dropped. Dividing top and bottom by k_{-1}, one gets the classical Rideal-Eley mechanism with Equation A-2 as the rate limiting step.

$$\gamma_o = 2k_2K[O]/(1+K[O]) \quad \text{A-31}$$

where K is the equilibrium constant for Reaction A-1.

Another assumption assumes that oxygen atom density is approximately constant near the surface and oxygen atom density can, therefore, be combined with the preexponential constants of the Arrhenius equation:

$$\gamma_o = 2k_2K/(1+K) \qquad \text{A-32}$$

This is the simplest 4 parameter model possible.

$$\text{where } k_2 = k_{20} \exp(-Ea/k_BT) \qquad \text{A-33}$$

$$\text{and } K = Ka \exp(D/K_BT). \qquad \text{A-34}$$

Note: In the report, R, the universal gas constant, is used in place of k_B.

APPENDIX B

Derivation of a Langmuir Hinshelwood Mechanistic Model

The basic rate equations are:

Adsorption of oxygen onto the surface

$$O + [S] \underset{k_{-1}}{\overset{k_1}{\rightleftharpoons}} [OS] \qquad \text{B-1}$$

Reaction of 2 surface oxygens to form molecular oxygen

$$[OS] + [OS] \longrightarrow O_2 + 2[S] \qquad \text{B-2}$$

In this derivation Reaction, B-1 is assumed in pseudo-equilibrium and Reaction B-2 is rate limiting, thus:

$$d\ O_2/A_N dt = k_2[OS]^2 \qquad \text{B-3}$$

and

$$k_1[O][S]=k_{-1}[OS] \qquad \text{B-4}$$

If the number of total surface sites are constant, then:

$$[S_0]=[S]+[OS] \qquad \text{B-5}$$

or

$$[S]=[S_0]-[OS] \qquad \text{B-6}$$

Substitution of Equation B-6 into Equation B-4 leads to the following equation:

$$k_1[O][S_0]=k_{-1}[OS]+k_1[O][OS] \qquad \text{B-7}$$

or solving for [OS],

$$[OS]= k_1[O][S_0]/(k_{-1}+k_1[O]) \qquad \text{B-8}$$

Multiply top and bottom by k_{-1} and define K to be the equilibrium constant, Equation B-8 becomes:

$$[OS]=K[O][S_0]/(1+K[O]) \qquad \text{B-9}$$

Substitution of Equation B-9 into Equation B-3 leads to:

$$dO_2/A_N dt=k_2K^2[O]^2/(1+K[O])^2 \qquad \text{B-10}$$

From Appendix A above,

$$2\ dO_2/dt=-dO/dt \qquad \text{B-11}$$

and

$$N_O=[O][k_BT/2m\pi]^{1/2} \qquad \text{B-12}$$

thus,

$$\gamma_o=2\ k_2[2m\pi/k_BT]^{1/2}K^2[O]/(1\ +\ K[O])^2 \qquad \text{B-13}$$

The rate constant, k_2 and equilibrium constant, K, follow Arrhenius equations.

$$k_2=k_{20}\ \exp\ (-Ea/k_BT) \qquad \text{B-14}$$

$$K=Ka\ \exp\ (D/k_BT) \qquad \text{B-15}$$

APPENDIX C

Data Base Used in the Study

		Nitrogen Data					Nitrogen Data		
Gas		Nitrogen	Nitrogen	Nitrogen	Nitrogen	Nitrogen	Nitrogen	Nitrogen	Nitrogen
Resv. Pres.	N/m2	137900	137900	137900	137900	137900	137900		
Arc Current	Amps	1200	1200	1200	1200	1200	1200	1600	750
Area Ratio		144	144	400	400	400	400		
Nozzle Angle		30	30	30	30	30	30		
Stag. Pres.	N/m2	2840	2840	810	810	810	810	2610	965
Enth. B.L.	MJ/kg	27.9	27.9	27.9	27.9	27.9	27.9	12.7	32.2
Mach #, F.S.		5.4	5.4	7.1	7.1	7.1	7.1	17.2	7.4
Temp., F.S	K	2920	2920	1800	1800	1800	1800	60	500
N mole fract.	F.S.	0.40	0.40	0.40	0.40	0.40	0.40	0.24	0.77
O mole fract.	F.S.	0.00	0.00	0.00	0.00	0.00	0.00	NA	NA
Temp., B.L.	K	5980	5980	5640	5640	5640	5640		
N mole fract.	B.L.	0.73	0.73	0.75	0.75	0.75	0.75	0.39	0.87
O mole fract.	B.L.	0.00	0.00	0.00	0.00	0.00	0.00		
model		hemi	flat	cone	hemi	flat	flat	flat	flat
material		FRCI-20RCG	FRCI-20RCG	FRCI-20RCG	FRCI-20RCG	FRCI-20RCG	FRCI-20RCG	HRSI-RCG	HRSI-RCG
z-dist.	cm	10	10	10	10	10	10	11.6	11.6
Model Rad.	cm	5.08	3.81	2.54	5.08	3.81	5.08	5.08	5.08
Surf.Ht. Flux	W/cm2	64.3	46.5	40.8	33.3	23.4	20.7	39.60	38.90
Temp, Wall	K	1889	1742	1686	1603	1467	1422	1668	1661
1000/Tw		0.5294	0.5741	0.5931	0.6238	0.6817	0.7032	0.5995	0.6020
Part. Pres.		2073	2073	608	608	608	608	1010	840
Gamma N		0.00894	0.00943	0.01380	0.01465	0.01194	0.01068	0.01945	0.01478
Log(gamma N)		-2.0486	-2.0257	-1.8601	-1.8343	-1.9229	-1.9714	-1.7110	-1.8302
Source		1	1	1	1	1	1	2	2

Abbreviations:

B.L. Boundary Layer
F.S. Free Stream

Sources:

1. Kolodziej, P. and Stewart, D.A., AIAA-87-1637, 1987.
2. Scott, C.D., in Aero. & Planetary Entry ed. by A.L.Crosbie Vol 77., Prog. in Astro. and Aero. 1981, pp 192-212.
3. Stewart, D.A., Rakich, J.V., and Lanfranco, M.J., in Thermo. of Atomos Entry, ed. by T.E.Horton Vol 82, Prog. in Astro. and Aero., 1982, pp 248-272.
4. Willey, R.J. Summer Faculty Fellowship NASA-JSC, 1988.

5a. Marinelli, W.J., AIAA-88-2667, 1988.
5b. Marinelli, W.J. and Campbell, J.P. NAS9-17565, July 1986.

Nitrogen Data

Gas	Nitrogen	Nitrogen	Nitrogen	Nitrogen	Nitrogen	Nitrogen	Nitrogen	Nitrogen	Nitrogen
Resv. Pres.									
Arc Current	600	450	300	300	400	400	300	300	550
Area Ratio									144
Nozzle Angle									16
Stag. Pres.	951	1390	752	1190	896	465	827	427	839
Enth. B.L.	27.3	16.9	20.1	13.0	5.5	8.6	8.6	7.1	10.1
Mach #, F.S.	6.8	11.4	6.2	16.2	7.0	4.6	7.0	4.5	5.2
Temp., F.S	590	140	500	50	150	370	150	340	
N mole fract.	0.61	0.37	0.45	0.28	0.11	0.16	0.08	0.12	1
O mole fract.	NA	NA	NA	NA	NA	NA	NA	NA	0
Temp., B.L.									
N mole fract.	0.76	0.54	0.61	0.44	0.19	0.28	0.15	0.22	0.35
O mole fract.									
model	flat	flat	flat	flat	flat	flat	flat	flat	hemi
material	HRSI-RCG	HRSI-RCG	HRSI-RCG	HRSI-RCG	HRSI-RCG	HRSI-RCG	HRSI-RCG	HRSI-RCG	HRSI
z-dist.	11.6	11.6	11.6	11.6	11.6	11.6	11.6	11.6	3
Model Rad.	5.08	5.08	5.08	5.08	5.08	5.08	5.08	5.08	5.08
Surf.Ht. Flux	32.00	29.30	21.80	18.80	7.60	5.85	5.64	4.43	71.5
Temp, Wall	1582	1546	1438	1387	1092	1022	1014	996	1536
1000/Tw	0.6321	0.6468	0.6954	0.7210	0.9158	0.9785	0.9862	1.0040	0.6510
Part. Pres.	721	751	461	521	170	128	120	92	291
Gamma N	0.01740	0.01499	0.02155	0.01534	0.00943	0.00810	0.00772	0.00687	0.01504
Log(gamma N)	-1.7595	-1.8242	-1.6665	-1.8141	-2.0255	-2.0915	-2.1121	-2.1633	-1.8228
Source	2	2	2	2	2	2	2	2	4

Nitrogen Data

Gas	Nitrogen	Nitrogen	Nitrogen	Nitrogen	Nitrogen	Nitrogen	Nitrogen	Nitrogen	Nitrogen
Resv. Pres.									
Arc Current	550	525	500	501	501	451	402	400	400
Area Ratio	144	144	144	144	144	144	144	144	144
Nozzle Angle	16	16	16	16	16	16	16	16	16
Stag. Pres.	886	874	754	852	858	843	786	767	669
Enth. B.L.	9.8	9.4	9.3	9.1	9.1	8.5	7.8	7.7	7.7
Mach #, F.S.	5.2	5.1	5.1	5.1	5.1	5.1	5.1	5.1	5.0
Temp., F.S									
N mole fract.	1	1	1	1	1	1	1	1	1
O mole fract.	0	0	0	0	0	0	0	0	0
Temp., B.L.									
N mole fract.	0.33	0.32	0.34	0.31	0.31	0.28	0.26	0.27	0.27
O mole fract.									
model	hemi	hemi	hemi	hemi	hemi	hemi	hemi	hemi	hemi
material	HRSI	HRSI	HRSI	HRSI	HRSI	HRSI	HRSI	HRSI	HRSI
z-dist.	3	3	3	3	3	3	3	3	3
Model Rad.	5.08	5.08	5.08	5.08	5.08	5.08	5.08	5.08	5.08
Surf.Ht. Flux	68.2	66.9	67.5	64.4	61.8	60.1	50.1	53.7	50.9
Temp, Wall	1524	1506	1496	1493	1490	1460	1412	1411	1402
1000/Tw	0.6562	0.6640	0.6685	0.6697	0.6711	0.6849	0.7084	0.7088	0.7132
Part. Pres.	295	279	257	268	266	240	205	208	180
Gamma N	0.01401	0.01267	0.01723	0.01464	0.01527	0.01156	0.01383	0.01437	0.01368
Log(gamma N)	-1.8536	-1.8972	-1.7637	-1.8345	-1.8162	-1.9370	-1.8592	-1.8425	-1.8639
Source	4	4	4	4	4	4	4	4	4

Nitrogen Data

Gas	Nitrogen	Nitrogen
Resv. Pres.		
Arc Current	401	
Area Ratio	144	
Nozzle Angle	16	
Stag. Pres.	747	
Enth. B.L.	7.9	
Mach #, F.S.	5.1	
Temp., F.S		
N mole fract.	1	
O mole fract.	0	
Temp., B.L.		
N mole fract.	0.28	
O mole fract.		
model	hemi	
material	HRSI	HRSI
z-dist.	3	
Model Rad.	5.08	
Surf.Ht. Flux	42.2	
Temp, Wall	1350	300
1000/Tw	0.7408	3.3333
Part. Pres.	207	133
Gamma N	0.01540	0.00019
Log(gamma N)	-1.8125	-3.7212
Source	4	5b

	Units			Oxygen Data			Oxygen Data		
Gas		Air	Air	Air	Air	Air	Air	Air	Air
Resv. Pres.	N/m2	137900	275800	275800	137900	137900	275800	137900	137900
Arc Current	Amps	1200	1600	1600	1200	1200	1600	1200	1200
Area Ratio		144	400	400	144	400	400	400	400
Nozzle Angle		30	30	30	30	30	30	30	30
Stag. Pres.	N/m2	2840	1420	1420	2840	810	1420	810	810
Enth. B.L.	MJ/kg	23.3	23.3	23.3	23.3	23.3	23.3	23.3	23.3
Mach #, F.S.		5.8	7.7	7.7	5.8	7.5	7.7	7.5	7.5
Temp., F.S	K	2510	1460	1460	2510	1500	1460	1500	1500
N mole fract.	F.S.	0.09	0.08	0.08	0.09	0.09	0.08	0.09	0.09
O mole fract.	F.S.	0.36	0.36	0.36	0.36	0.36	0.36	0.36	0.36
Temp., B.L.	K	5710	5540	5540	5710	5400	5540	5400	5400
N mole fract.	B.L.	0.45	0.45	0.45	0.45	0.46	0.45	0.46	0.46
O mole fract.	B.L.	0.29	0.29	0.29	0.29	0.29	0.29	0.29	0.29
Model		hemi	cone	hemi	flat	cone	flat	hemi	flat
Material		FRCI-20RCG	FRCI-20RCG	FRCI-20RCG	FRCI-20RCG	FRCI-20RCG	FRCI-20RCG	FRCI-20RCG	FRCI-20RCG
z-dist.	cm	10	10	10	10	10	10	10	10
Model Rad.	cm	5.08	2.54	5.08	3.81	2.54	3.81	5.08	3.81
Surf.Ht. Flux	W/cm2	56.7	53.6	46.5	44.8	36.9	34.5	32.4	22.3
Temp, Wall	K	1831	1806	1742	1726	1644	1617	1592	1450
1000/Tw		0.5461	0.5537	0.5741	0.5794	0.6083	0.6184	0.6281	0.6897
Part. Pres.	Pa	824	412	412	824	235	412	235	235
Gamma 0		0.0037	0.0101	0.0189	0.0052	0.0107	0.0097	0.0306	0.0179
log(gamma)		-2.4318	-1.9971	-1.7229	-2.2800	-1.9714	-2.0143	-1.5143	-1.7471
Source		1	1	1	1	1	1	1	1

Oxygen Data

Gas	Air	Air	Air	Air	Air	Air	Air	Air	Air
Resv. Pres.									
Arc Current	800	400	250			401	400	450	425
Area Ratio						144	144	144	144
Nozzle Angle						16	16	16	16
Stag. Pres.	1510	1320	1170	2000	1400	860	888	909	905
Enth. B.L.	22.4	15.7	12.0	16	13.95	8.3	8.0	9.1	8.7
Mach #, F.S.	7.8	7.6	7.1	6	5.75	5.5	5.2	5.4	5.5
Temp., F.S	500	440	420						
N mole fract.	(0.47)	(0.27)	(0.17)						
O mole fract.	(0.23)	(0.23)	(0.23)						
Temp., B.L.									
N mole fract.									
O mole fract.	0.25	0.28	0.30	0.23	0.29	0.28	0.15	0.28	0.28
Model	flat	flat	flat			hemi	hemi	hemi	hemi
Material	HRSI-RCG	HRSI-RCG	HRSI-RCG		RCG	HRSI	HRSI	HRSI	HRSI
z-dist.	12	12	12			3	3	3	3
Model Rad.	5.08	5.08	5.08		5	5.08	5.08	5.08	5.08
Surf.Ht. Flux	37.5	26.7	20.1			69.2	65.1	64.4	60.1
Temp, Wall	1647	1493	1419	1556	1344	1557	1552	1540	1527
1000/Tw	0.6072	0.6700	0.7047	0.6427	0.7440	0.6422	0.6442	0.6494	0.6548
Part. Pres.	370	368	351	451	406	241	134	252	253
Gamma 0	0.0236	0.0130	0.0077	0.0173	0.0112	0.0089	0.0279	0.0089	0.0108
log(gamma)	-1.6269	-1.8859	-2.1109	-1.7611	-1.9508	-2.0520	-1.5540	-2.0530	-1.9660
Source	2	2	2	3	3	4	4	4	4

Oxygen Data

Gas	Air	Air	Air	Air	Air	Air	Air	Air	Air
Resv. Pres.									
Arc Current	376	426	401	403	375	326	350	300	350
Area Ratio	144	144	144	144	144	144	144	144	144
Nozzle Angle	16	16	16	16	16	16	16	16	16
Stag. Pres.	844	869	847	854	818	817	794	801	814
Enth. B.L.	7.8	8.7	8.3	8.2	7.8	7.0	7.3	6.4	7.3
Mach #, F.S.	5.2	5.5	5.5	5.5	5.5	5.2	5.5	5.3	5.5
Temp., F.S									
N mole fract.									
O mole fract.									
Temp., B.L.									
N mole fract.									
O mole fract.	0.15	0.28	0.28	0.28	0.28	0.16	0.28	0.15	0.28
Model	hemi	hemi	hemi	hemi	hemi	hemi	hemi	hemi	hemi
Material	HRSI	HRSI	HRSI	HRSI	HRSI	HRSI	HRSI	HRSI	HRSI
z-dist.	3	3	3	3	3	3	3	3	3
Model Rad.	5.08	5.08	5.08	5.08	5.08	5.08	5.08	5.08	5.08
Surf.Ht. Flux	60.9	63.7	56.6	60.1	52.5	52.9	47.6	52.0	50.7
Temp, Wall	1522	1518	1501	1497	1486	1479	1458	1456	1449
1000/Tw	0.6570	0.6587	0.6664	0.6679	0.6730	0.6761	0.6858	0.6868	0.6903
Part. Pres.	127	241	237	239	230	128	225	124	231
Gamma 0	0.0164	0.0082	0.0152	0.0084	0.0215	0.0197	0.0243	0.0115	0.0150
log(gamma)	-1.7860	-2.0880	-1.8170	-2.0770	-1.6680	-1.7050	-1.6140	-1.9410	-1.8240
Source	4	4	4	4	4	4	4	4	4

Gas	Oxygen
Resv. Pres.	
Arc Current	
Area Ratio	
Nozzle Angle	
Stag. Pres.	
Enth. B.L.	
Mach #, F.S.	
Temp., F.S	
N mole fract.	
O mole fract.	
Temp., B.L.	
N mole fract.	
O mole fract.	
Model	
Material	HRSI
z-dist.	
Model Rad.	
Surf.Ht. Flux	
Temp, Wall	300
1000/Tw	3.3333
Part. Pres.	133
Gamma 0	0.0002
log(gamma)	-3.6990
Source	5